Title
Chemical and genetic perturbations reveal wiring of the protein homeostasis network in prostate cancer

Author
Shkedi, Arielle

Publication Date
2021

Peer reviewed|Thesis/dissertation

Chemical and genetic perturbations reveal wiring of the protein homeostasis network in prostate cancer

by
Arielle Shkedi

DISSERTATION
Submitted in partial satisfaction of the requirements for degree of
DOCTOR OF PHILOSOPHY

in

Pharmaceutical Sciences and Pharmacogenomics

in the

GRADUATE DIVISION
of the
UNIVERSITY OF CALIFORNIA, SAN FRANCISCO

Approved:

DocuSigned by:
Jason Gestwicki
4909848DBB404E5...

Jason Gestwicki
Chair

DocuSigned by:
LUKE GILBERT
DocuSigned by:
Davide Ruggero
14C3B6AD60C5446...

LUKE GILBERT

Davide Ruggero

Committee Members

Acknowledgements

I have many people to thank and acknowledge for helping me through my graduate career. First, I would like to think my mentor Dr. Jason Gestwicki, and his lab, for providing me with great support for the past five years. You are all amazingly dedicated scientists who have helped me grow and shaped my professional interests and abilities. In particular, I would like to thank Isabelle Taylor, Taylor Arhar, Meredith Kuo, Hao Shao, Cory Nadel, Kelly Montgomery, and Oleta Johnson. You all provided both scientific and emotional support, and I owe much of my success to you. I would also like to thank my thesis committee, Drs. Luke Gilbert and Davide Ruggero, for their valuable advice and feedback, and my undergraduate professor Dr. Chris Nicchitta for showing me how to do scientific research and pushing me to study biology.

I would also like to thank my family for their constant love and encouragement. My parents, Naomi and Yehuda Shkedi, always pushed me to do my best and supported my scientific interests, even when they didn't understand the work I was doing. My sister Michelle and brother-in-law Tudor have also been extremely supportive, and I am so lucky that we were able to live in San Francisco together. I would also like to thank my grandmother Miriam Lilo, and the rest of my family in Israel.

Lastly, I would like to thank my boyfriend Evan Fuller, and my other friends, from graduate school, undergraduate, and beyond. Evan, it feels fitting that I met you right before my qualifying exam, so you have been with me almost every step of the way in my PhD. To my PSPG friends, I'm so proud to have gone through graduate school

together, and I can’t wait to see what we all accomplish. And a special shout-out to Serena Tamura for especially helping me transition into a working adult. Lastly, to my friends from Duke, Erica, Jenna, Amanda, and Jules, thanks for being such amazing friends and finding ways to come visit, even when it wasn’t easy. To all my other family, friends, and colleagues, you played a huge role in my achievements as well, so thank you for your unconditional support.

Contributions

Chapter 2: The RNA-seq and data analysis presented in this chapter were performed by the Genomics Core at UCSF, including Michael Adkisson, Andrew Shroeder, and Walter L. Eckalbar. Additionally, Meredith (Szu-Yu) Kuo, PhD aided in the design and implementation of the high-throughput drug combination screens.

Chapter 3: The functional genomics shRNA screens presented in this chapter were performed by Isabelle Taylor, PhD. The metabolic assays were conducted by Frank Echtenkamp, PhD. The multiple myeloma validation was conducted by Poornima Ramkumar, PhD, and the Hsp60 gene expression evaluation was performed by Mohamed Alshalalfa.

Chemical and genetic perturbations reveal wiring of the protein homeostasis network in prostate cancer

Arielle Shkedi

Abstract

The protein homeostasis (proteostasis) network is composed of multiple components and pathways that work together to govern protein production, folding, stability and degradation. Cancer cells are especially dependent on the proteostasis network, due to their high protein load, genomic instability, and oncogenic signaling pathways. For this reason, inhibitors of the proteostasis network have been developed as anti-cancer therapies, with varying success. In this dissertation, I will discuss two adjacent strategies we employed to better understand wiring of the proteostasis network in cancer cells. In this first approach, we used existing chemical inhibitors of various proteostasis targets, such as molecular chaperones and the proteasome, and tested them in combination to reveal patterns of synergy and antagonism. In the second approach, we used a functional genomics shRNA screening approach to probe at genetic vulnerabilities in the proteostasis network and identify new targets. In both these studies, we focused our work on prostate cancer, due to it's established dependence on molecular chaperones. Through these approaches we were able to identify both synergistic drug combinations and new proteostasis targets that can be further explored as anti-cancer therapeutic strategies. Furthermore, we gained a better understanding of proteostasis network wiring in prostate cancer cells, which provides broader insights into how to can be therapeutically targeted in cancer.

Table of Contents

List of Figures

List of Tables

Chapter 1: Introduction

Introduction

The proteostasis network is a highly conserved set of pathways that balances the synthesis, folding, activation, and degradation of the proteome (*1*). There are hundreds of components dedicated to this network, including molecular chaperones (*e.g.* heat shock proteins), co-chaperones, the translation machinery, the ubiquitin-proteasome system and autophagy-lysosome pathway (*2, 3*). This network is characterized by major "nodes" that are connected, often through direct protein-protein interactions, with the other components (*4*). Importantly, flux of proteins through the network is tightly regulated by stress signaling, including the unfolded protein response (UPR), the integrated stress response (ISR), the heat shock response (HSR) and others (*5-8*). Specifically, stress signaling elevates the levels of proteostasis factors, such as some chaperones, as well as tuning the rates of protein synthesis and turnover, allowing cells to adapt to changing conditions. Thus, the proteostasis network is both interconnected and responsive, likely allowing different subnetworks to play dominant roles in response to specific perturbations (*9*).

Cancer cells have been found to be particularly reliant on specific components of the proteostasis network, likely because of the rapid growth, high frequency of translation errors and genomic instability of these cells(*10, 11*). For example, major nodes of the proteostasis network, such as Hsp70, Hsp90 and HSF1, are important for maintaining tumorigenesis (*7, 12, 13*). In contrast, normal, untransformed cells seem to be less reliant on these same proteostasis factors, perhaps because their networks are more robust to the loss of an individual component. The mechanistic reasons for differential vulnerability are often not clear, but recent studies have started to provide insights. For

example, Hsp90 binds to a distinct set of co-chaperones in cancer cells vs. non-transformed cells(*14*),(*15*), suggesting that the same node can be "wired" differentially following tumorigenesis.

These observations, and others, have led to the hypothesis that nodes of the proteostasis network are promising drug targets, which could be exploited for anti-cancer therapy (*16-19*). Accordingly, substantial efforts have been mobilized to create chemical inhibitors of proteostasis targets (*20-22*). Although this remains an active research area, a subset of these molecules have advanced to the clinical setting, with varying levels of success. For example, proteasome inhibitors are approved and widely used in treating multiple myeloma(*23*). However, inhibitors of other proteostasis targets have been less successful(*24-26*), often due to lack of efficacy, rapid onset of resistance and/or unacceptable toxicity. Moreover, even proteasome inhibitors are ineffective at treating other cancer subtypes, such as solid tumors, for reasons that remain uncertain (*27*).

The success of proteasome inhibitors shows that targeting the proteostasis network is a viable option for anti-cancer therapy, but many questions still remain. In this thesis, I will describe two studies performed to better understand cancer cell dependence and wiring on the proteostasis network. The first study involved probing the network with well-established proteostasis inhibitors in combination, to understand how cancer cells responded to dual-proteostasis inhibition. This is especially important because as described, the network is highly dynamic and readily able to compensate for loss of function at specific nodes. Through these studies, we were able to identify synergistic

and antagonistic combinations of proteostasis inhibitors that have larger implications for potential therapeutic strategies. In the second study, we genetically perturbed the proteostasis inhibitor using a functional genomics shRNA screen, to identify weaknesses. Through this work, we identified a new target, the mitochondrial chaperone Hsp60, that shows promise as an anti-cancer target in prostate cancer cells. Together, these two chapters show the important role that the proteostasis network has in cancer cell growth and survival, and highlights how we can use chemical and genetic tools to disrupt the network to find new targets and improve our use of existing inhibitors.

References

1. E. T. Powers, R. I. Morimoto, A. Dillin, J. W. Kelly, W. E. Balch, Biological and chemical approaches to diseases of proteostasis deficiency. *Annu Rev Biochem* **78**, 959-991 (2009).
2. C. Voisine, J. S. Pedersen, R. I. Morimoto, Chaperone networks: tipping the balance in protein folding diseases. *Neurobiol Dis* **40**, 12-20 (2010).
3. J. Labbadia, R. I. Morimoto, The biology of proteostasis in aging and disease. *Annu Rev Biochem* **84**, 435-464 (2015).
4. R. Freilich, T. Arhar, J. L. Abrams, J. E. Gestwicki, Protein-Protein Interactions in the Molecular Chaperone Network. *Acc Chem Res* **51**, 940-949 (2018).
5. Y. Liu, Y. Ye, Proteostasis regulation at the endoplasmic reticulum: a new perturbation site for targeted cancer therapy. *Cell research* **21**, 867-883 (2011).
6. L. Whitesell, R. Bagatell, R. Falsey, The stress response: implications for the clinical development of hsp90 inhibitors. *Curr Cancer Drug Targets* **3**, 349-358 (2003).
7. C. Dai, L. Whitesell, A. B. Rogers, S. Lindquist, Heat shock factor 1 is a powerful multifaceted modifier of carcinogenesis. *Cell* **130**, 1005-1018 (2007).
8. K. Pakos-Zebrucka *et al.*, The integrated stress response. *EMBO Rep* **17**, 1374-1395 (2016).
9. S. Joshi *et al.*, Adapting to stress - chaperome networks in cancer. *Nature reviews* **18**, 562-575 (2018).

10. P. Workman, F. Burrows, L. Neckers, N. Rosen, Drugging the cancer chaperone HSP90: combinatorial therapeutic exploitation of oncogene addiction and tumor stress. *Ann N Y Acad Sci* **1113**, 202-216 (2007).
11. S. K. Calderwood, J. Gong, Heat Shock Proteins Promote Cancer: It's a Protection Racket. *Trends Biochem Sci*, (2016).
12. L. Whitesell, S. Lindquist, Inhibiting the transcription factor HSF1 as an anticancer strategy. *Expert Opin Ther Targets* **13**, 469-478 (2009).
13. V. L. Gabai *et al.*, Anticancer Effects of Targeting Hsp70 in Tumor Stromal Cells. *Cancer Res* **76**, 5926-5932 (2016).
14. A. Hadizadeh Esfahani, A. Sverchkova, J. Saez-Rodriguez, A. A. Schuppert, M. Brehme, A systematic atlas of chaperome deregulation topologies across the human cancer landscape. *PLoS computational biology* **14**, e1005890 (2018).
15. A. Rodina *et al.*, The epichaperome is an integrated chaperome network that facilitates tumour survival. *Nature* **538**, 397-401 (2016).
16. C. G. Evans, L. Chang, J. E. Gestwicki, Heat shock protein 70 (hsp70) as an emerging drug target. *J Med Chem* **53**, 4585-4602 (2010).
17. H. Urra, E. Dufey, T. Avril, E. Chevet, C. Hetz, Endoplasmic Reticulum Stress and the Hallmarks of Cancer. *Trends Cancer* **2**, 252-262 (2016).
18. L. Ruan *et al.*, Mitochondria-Associated Proteostasis. *Annu Rev Biophys* **49**, 41-67 (2020).
19. P. Workman, M. V. Powers, Chaperoning cell death: a critical dual role for Hsp90 in small-cell lung cancer. *Nat Chem Biol* **3**, 455-457 (2007).

20. B. Dong *et al.*, Targeting therapy-resistant prostate cancer via a direct inhibitor of the human heat shock transcription factor 1. *Science translational medicine* **12**, (2020).

21. S. J. Mishra *et al.*, The Development of Hsp90beta-Selective Inhibitors to Overcome Detriments Associated with pan-Hsp90 Inhibition. *J Med Chem* **64**, 1545-1557 (2021).

22. D. J. Anderson *et al.*, Targeting the AAA ATPase p97 as an Approach to Treat Cancer through Disruption of Protein Homeostasis. *Cancer cell* **28**, 653-665 (2015).

23. E. E. Manasanch, R. Z. Orlowski, Proteasome inhibitors in cancer therapy. *Nat Rev Clin Oncol* **14**, 417-433 (2017).

24. G. Garg, A. Khandelwal, B. S. Blagg, Anticancer Inhibitors of Hsp90 Function: Beyond the Usual Suspects. *Adv Cancer Res* **129**, 51-88 (2016).

25. S. Chatterjee, S. Bhattacharya, M. A. Socinski, T. F. Burns, HSP90 inhibitors in lung cancer: promise still unfulfilled. *Clin Adv Hematol Oncol* **14**, 346-356 (2016).

26. A. R. Goloudina, O. N. Demidov, C. Garrido, Inhibition of HSP70: a challenging anti-cancer strategy. *Cancer letters* **325**, 117-124 (2012).

27. Z. Huang *et al.*, Efficacy of therapy with bortezomib in solid tumors: a review based on 32 clinical trials. *Future oncology* **10**, 1795-1807 (2014).

Chapter 2: Inhibitor Combinations Reveal Wiring of the Proteostasis Network in Prostate Cancer Cells

Abstract

The protein homeostasis (proteostasis) network is composed of multiple components and pathways that work together to balance protein production, folding, stability and turnover. Cancer cells are particularly reliant on this network, which has led to inhibitors of proteostasis targets being pursued as anti-cancer therapies. However, the proteostasis network is highly inter-connected, and it is hypothesized that inhibition of one node might lead to compensation by other parts of the network. To better understand the implications of these connections on potential treatment strategies, we dosed 22Rv1 prostate cancer cells with inhibitors of four major proteostasis targets (Hsp70, Hsp90, proteasome and p97), either alone or in binary combinations, and measured effects on cell growth. The results reveal a series of additive, synergistic and antagonistic relationships, including strong synergy between inhibitors of p97 and the proteasome, and striking antagonism between inhibitors of Hsp90 and the proteasome. Based on RNA-seq, these relationships are associated, in part, with activation of stress pathways. To probe the generality of these findings in prostate cancer, we repeated the inhibitor screens in three additional cell lines, revealing that some relationships, such as the Hsp90-proteasome antagonism, are common to all the cells, while others are cell-line specific. Together, these results suggest that cocktails of proteostasis inhibitors might be a powerful way of treating some cancers, although antagonism that blunts the efficacy of both molecules is also possible.

Introduction

As discussed, the proteostasis network has many roles in tumorigenesis, and has been shown to be a viable target for anti-cancer therapeutics. However, in the clinic, proteostasis inhibitors have had mixed results. One hypothesis to explain the uneven and sometimes confounding clinical results is that the interconnected nature of the proteostasis network might create opportunities for compensation by stress responses (*1*). For example, it is well established that treatment with Hsp90 inhibitors, at least those that bind the N-terminal domain, leads to elevated expression of Hsp70 and other chaperones (*2*). Similarly, proteasome inhibitors induce autophagy (*3*), and inhibition of p97 activates the UPR (*4*). Mounting evidence suggests that these compound-induced stress responses might directly contribute to inhibitor resistance. For example, activation of autophagy and other stress pathways (*1*), makes certain cancer cells relatively resistant to Hsp70 inhibition (*5*). Additionally, activation of the HSR has been linked to bortezomib resistance in multiple myeloma (*6*)[,](*7*). Thus, cancer cells seem to activate stress pathways in response to proteostasis inhibitors, which can, in some cases, provide them with partial protection.

Because the nodes of the proteostasis network are inter-connected and subject to regulation by stress responses, combinations of proteostasis inhibitors might, in some cases, be strongly synergistic (*8*). Specifically, inhibition of two proteostasis targets simultaneously might limit the ability of cancer cells to circumvent loss of one target during single-agent treatments. However, while some promising combinations have been proposed (*9*-*11*), this possibility has not been systematically explored. Here, we

tested four proteostasis inhibitors by themselves and in binary combinations to reveal additive, synergistic and antagonistic relationships. We chose to perform these screens in 22Rv1 prostate cancer cells, given the known reliance of these cells on the proteostasis network (*12, 13*). As test compounds, we selected four well-known inhibitors that target major nodes in the proteostasis network: Hsp70, Hsp90, the 26S proteasome and VCP/p97. Briefly, Hsp70 and Hsp90 are molecular chaperones involved in protein folding and activation (*14*). VCP/p97 is a AAA^+ ATPase which plays multiple roles in protein trafficking and quality control (*15*), and the 26S proteasome is responsible for degrading ubiquitinated proteins (*16*). Beyond their individual functions, these nodes also have well-known functional relationships within a shared sub-network (**Figure 2.1a**). For example, Hsp70 delivers unfolded proteins to Hsp90 through a shared co-chaperone, Hop (*17, 18*). Moreover, p97 collaborates with Hsp70 and the proteasome during ER-associated degradation (ERAD) (*19, 20*) and both Hsp70 and Hsp90 are involved in delivering proteins to the proteasome for degradation (*21, 22*). Thus, we were interested in whether inhibitors of one node in this particular sub-network might create synergy with inhibitors of others.

To target these four nodes, we selected well-characterized chemical inhibitors: JG-98 (Hsp70 inhibitor) (*23*), 17-DMAG (Hsp90 inhibitor) (*24*), bortezomib (proteasome inhibitor) (*25*) and CB-5083 (p97 inhibitor) (*4*) (**Figure 2.1b**). These compounds were selected because three of them have been explored in clinical trials, while the fourth, JG-98, is a close analog of a molecule, MKT-077, tested in Phase I (*26*). Using a high throughput, 384-well growth assay, we tested binary combinations of the compounds on

growth of 22Rv1 prostate cancer cells, revealing examples of both synergy (Hsp70-Hsp90, p97-Hsp90, p97-proteasome) and antagonism (Hsp70-proteasome, Hsp90-proteasome). Transcriptome studies on cells treated with select combinations revealed differences in the cellular stress response(s) compared to the single agent treatments, perhaps underlying the observed synergy/antagonism. Also, repeating these screens in three additional prostate cancer cell lines, C4-2, LNCaP and PC3, identified both shared and cell-type specific relationships, suggesting that the "wiring" of the proteostasis network can partially differ across cell lines. Together, these studies show that testing proteostasis inhibitor combinations in cultured cells reveals patterns of additivity, synergy and antagonism, which could aid in the design (or avoidance) of therapeutic combinations for use in the clinic.

Results

Proteostasis inhibitors reduce cell viability in 22Rv1 prostate cancer cells, as single agents. To provide a baseline for combination studies, we first confirmed the effects of the four proteostasis inhibitors: JG-98 (Hsp70 inhibitor), 17-DMAG (Hsp90 inhibitor), bortezomib (proteasome inhibitor) and CB-5083 (p97 inhibitor) on growth of 22Rv1 cells as single agents. After a 72-hour treatment, each of the inhibitors, but not the DMSO control, reduced growth of 22Rv1 cells, with IC_{50} values varying from 0.02 to 3.3 μM (**Figure 2.1b**). Consistent with literature observations, inhibitors of Hsp70, p97, and the proteasome reduced cell viability to nearly baseline at the highest doses, while Hsp90 inhibition produced a ~50% reduction, even at the highest concentrations.

Combination treatments reveal patterns of additivity, synergy and antagonism upon proteostasis disruption. Based on the calculated IC_{50} values, we then choose compound concentration ranges for use in the combination screens (see Methods). First, 22Rv1 cells were plated in 384-well plates, and, on the following day, compounds were added using standard laboratory automation. Treatments were performed in quadruplicate (4 wells per treatment) and each compound was tested in 8 concentrations (DMSO control, plus 7 doses in 2-fold dilutions; **Figure 2.2**). After 3 days of treatment, cell viability was quantified using Cell Titer Glo. From the resulting data, all of the values in the 8x8 treatment matrix were used to calculate synergy values using the ZIP synergy model (*27*) (**Figure 2.2**). There are multiple methods for estimating potential synergy or antagonism between compounds (*28, 29*) and consensus in which approach to select has been elusive (*30, 31*). In this case, we chose to use ZIP synergy because it utilizes the entire dose-response landscape (**Figure 2.2**, **Figure 2.3**), ensuring that all of the doses are represented when determining the numerical synergy value. This feature was especially important here because the Hsp90 inhibitor 17-DMAG did not reduce viability to baseline, which could create misleading synergy values if other approaches were employed. In this study, we considered scores to be additive if they were between the values of +1.5 and -1.5, while scores greater than +1.5 were categorized as synergistic and those less than -1.5 were antagonistic. We arrived at these arbitrary cutoff values by comparing the variance of the ZIP synergy scores across replicates and by manually examining the dose-response curves (see below). Importantly, this protocol and analysis pipeline was reproducible, with independent replicates on different days showing high correlation (**Figure 2.4**).

From the combination screens in 22Rv1 cells, we observed clear patterns of additivity, synergy and antagonism between the proteostasis inhibitors. For example, the combination of Hsp70 and p97 inhibitors was additive (ZIP score ~ 1.2), as co-treatment with the p97 inhibitor did not significantly impact the apparent IC_{50} of the Hsp70 inhibitor (**Figure 2.3**). However, other combinations, such as Hsp90-p97, Hsp90-Hsp70 and proteasome-p97, were synergistic. The combinations of Hsp90-p97 and Hsp70-Hsp90 were modestly synergistic (ZIP scores between +2.4 and +2.8), while the combination of p97 and proteasome inhibitor (compounds bortezomib and CB-5083) was the most synergistic, with a ZIP score of +9.1. This relationship is illustrated by examining a subset of the dose response curves, in which bortezomib alone is able to decrease cell viability (**Figure 2.3**; black curve), but the apparent IC_{50} is strongly enhanced when CB-5083 is added (**Figure 2.3**; blue curves). These findings of strong synergy confirm the long-standing idea that targeting two proteostasis nodes might, in some cases, enhance cancer cell death.

In addition to synergistic combinations, we were surprised to observe combinations that were strongly antagonistic. For example, the Hsp70-proteasome combination was antagonistic (ZIP score -5.5). This effect seemed most prominent at the higher doses of Hsp70 inhibitor, as is clear from examination of a subset of dose-response curves that show that the proteasome inhibitor (**Figure 2.3**; black curves) becomes less effective when the cells are also dosed with an Hsp70 inhibitor (**Figure 2.3**; blue curves). More strikingly, we found that the combination of Hsp90 and proteasome inhibitors was

strongly antagonistic (ZIP score -19.9). In a representative series of results, addition of 17-DMAG (**Figure 2.3**; blue curves) clearly suppresses the anti-proliferative activity of bortezomib compared to this compound alone (**Figure 2.3**; black curve). Indeed, at the higher doses of the Hsp90 inhibitor, the anti-proliferative effects of the proteasome inhibitor are nearly abolished. Thus, some proteostasis combinations can be strongly antagonistic.

To provide additional insight, we repeated a subset of the combination treatments, replacing 17-DMAG for an alternative Hsp90 inhibitor, AUY-922. In those studies, we observed effects consistent with those obtained using 17-DMAG (**Figure 2.5a**), suggesting that anti-proliferative activities are, at least in part, a product of target biology and not specific to the compound. Next, we repeated the screens using a non-tumorigenic prostate cell line RWPE-1 and found no strong synergy between any drug combination (**Figure 2.5b**). Thus, the combinations did not seem to generally increase toxicity to cells, but rather, to enhance selectivity for 22Rv1 cancer cells over the non-tumorigenic cells. Finally, we wanted to ensure that the handling steps do not contribute to the observed synergy values, so we repeated the combinations by testing compounds against themselves. In those studies, we found no synergy or antagonism (**Figure 2.5c**), giving additional confidence in the screening platform.

Androgen receptor (AR) stability may explain some, but not all, drug synergies. We next wanted to explore possible mechanisms of synergy and/or antagonism in 22Rv1 cells. 22Rv1 cells are a prostate cancer cell line that is reliant on the androgen

receptor (AR) signaling (*32*). However, these cells are relatively resistant to anti-androgen therapy because they express both full length (FL) AR and splicing variants (ARv) associated with severe disease (*33*). AR and its variants are established clients of Hsp70 and Hsp90 (*12*) and inhibitors of these chaperones have been shown to promote degradation of AR and ARv (*12, 34*). Indeed, we confirmed that treatment with combinations of JG-98 and 17-DMAG leads to loss of FL and ARv in 22Rv1 cells (**Figure 2.6a**), reducing AR to ~10% of total and ARv to ~60% of total. Consistent with previous reports (*12*), the single agent treatments show that Hsp70 inhibition has a more dramatic effect on ARv, while Hsp90 inhibition preferentially destabilizes FL AR. Thus, Hsp70 and Hsp90 inhibitors may be synergistic because their co-treatment leads to lower levels of both AR and ARv, interrupting the AR signaling required for growth of these cells. However, AR stability did not explain all of the synergies. For example, treatment with the synergistic combination, p97-proteasome, did not alter either AR or ARv levels under the same conditions (**Figure 2.6b**). Likewise, AR stability did not correlate with synergy or antagonism after co-treatment with inhibitors of p97-Hsp70, Hsp70-proteasome, or Hsp90-proteasome, with no substantial differences between single-agents and combination treatments (**Figure 2.7**). Together, these results suggest that AR stability can be important, but that different mechanism(s) may be underlying drug synergy and antagonism in response to most of the combinations.

RNASeq experiments reveal downstream signaling differences between inhibitor combinations. To examine the downstream effects of proteostasis inhibition in an unbiased way, RNA-seq was used to identify transcriptional differences in the response

of 22Rv1 cells to compounds and their combinations. Based on the growth assays, we focused these studies on 9 treatment conditions: a DMSO control, Hsp70, Hsp90, p97, or proteasome inhibition alone, and the Hsp70-Hsp90, p97-proteasome, and Hsp90-proteasome combinations. These combinations were selected to sample both synergistic (Hsp70-Hsp90 and p97-proteasome) and antagonistic (Hsp90-proteasome) examples. In the RNASeq studies, compounds were tested at a single concentration, selected by considering both the IC_{50} values (see **Figure 2.1**) and the results from the ZIP synergy analysis (see Methods).

22Rv1 cells were treated for 6 hours with the indicated compounds in triplicate, after which RNA was extracted and RNA-seq was performed (see Methods). Read count data was analyzed by DeSeq2 and the top 100 variably expressed genes were hierarchically clustered and visualized (**Figure 2.8**). First, we noted that almost all of the biological replicates clustered together, suggesting a reproducible and specific transcriptional response to each treatment. The only outlier was the JG-98 and 17-DMAG combination, where one of the three replicates did not co-cluster. Then, we further subdivided the top 100 variably expressed genes across all the treatments into 5 clusters (Cluster 1-5) and examined them via gene ontology (GO) analysis (**Figure 2.9a**). Cluster 1 contains stress response genes, such as DDIT4 and SESN2, as well as ER stress response genes linked to the UPR, including HSPA5 (BiP, an ER Hsp70) and DDIT3 (CHOP). Cluster 2 contains many heat shock proteins and co-chaperones, including multiple Hsp70s (HSPA1B, HSPA1A, HSPB1, HSPH1, HSPA8), Hsp90s (HSP9-AA1, HSP90AB1), Hsp70 co-chaperones (DNAJA1 and BAG3), and ubiquitin

(UBB). These genes are known to be upregulated following Hsp90 inhibition, but we additionally found that this effect is exacerbated with combined Hsp90-proteasome inhibition (**Figure 2.8**). Qualitatively, this group of genes includes many hallmarks of the HSR(*35*). Thus, the Hsp90-proteasome combination might be antagonistic because the HSR pathway, induced by both Hsp90 and proteasome inhibition, may combine to suppress activity of both compounds.

Clusters 3 and 5 produced less well-defined GO terms, and their relevance will require additional study. However, we were interested to find that Cluster 4 contains exclusively mitochondrially expressed genes (**Figure 2.8**). The mitochondrial genome contains 37 genes, and we observed up-regulation of a significant portion following treatment with either JG-98 alone or the JG-98 and 17-DMAG combination. JG-98 has been shown to target mitochondrial Hsp70(*23, 36*), and it seems likely that, in these cells, it impacts mitochondrial proteostasis.

Immunoblotting validates RNA-seq results and highlights differences in stress response to proteostasis inhibition. To validate a subset of these RNASeq findings, we examined the protein levels of representative stress response effectors, BiP (marker of the UPR) and Hsp72 (marker of the HSR), following proteostasis inhibition in the treated 22Rv1 cells (**Figure 2.9b**). We also monitored the levels of Hsc70/HSPA8, which is typically more mildly upregulated in stress responses. After 24 hours of compound treatment, we observe BiP upregulation following inhibition of the proteasome or p97 and after treatment with the p97 inhibitor or the combinations of p97-

proteasome or Hsp90-proteasome inhibitors, which is consistent with the transcriptional response. In multiple myeloma cells, inhibitors of p97 have also been shown to activate the UPR, leading to elevated BiP levels(*4*). Additionally, we observed that Hsp72 is elevated following treatment with either the Hsp90 inhibitor, the proteasome inhibitor or the Hsp90-proteasome inhibitor combination (**Figure 2.9b**). Interestingly, the response to the combination was generally stronger than Hsp90 or proteasome inhibition alone, consistent with the RNASeq. Thus, one mechanism driving antagonism between Hsp90 and proteasome inhibitors may be the strong up-regulation of HSR genes, which might blunt the activity of both compounds.

Additional prostate cancer cell lines have both similar and distinct patterns of proteostasis inhibitor sensitivity. Lastly, we probed how these patterns of drug synergy/antagonism might compare across other prostate cancer cell lines. To complement the studies in 22Rv1 cells, we repeated the combination screens in three additional cell lines: LNCaP, C4-2, and PC-3. Briefly, LNCaP cells are an androgen-sensitive prostate cell line, and C4-2 cells are an androgen insensitive cell line derived from LNCaPs. Like 22Rv1 cells, both LNCaPs and C4-2 express and are driven by AR signaling. PC-3 cells are a prostate line that are androgen-insensitive and do not express AR. We chose to screen these cell lines in addition to the androgen-insensitive 22Rv1 cells to get a broader picture of proteostasis combination synergies across a range of prostate cancer cell types with different origins, AR status and compound sensitivities.

We treated the three cell lines with an 8x8 matrix of compounds and summarized the resulting additivity, synergy and antagonism through calculation of ZIP synergy scores. In Figure 2.10, we also repeat the 22Rv1 results for clarity and comparison. Together, the results revealed that there are some similarities across the prostate cancer cell lines, but that none of them respond exactly the same way (**Figure 2.10a**). Among the similarities, the combination of Hsp70-p97 inhibitors tended to be synergistic (ZIP values+1.2 to 3.2) and the combination of Hsp90-proteasome inhibitors was always antagonistic (ZIP synergy between -6.9 and -19.9). The shared, antagonistic response to combinations of Hsp90 and proteasome inhibitors was especially intriguing. Examination of a subset of the dose response curves from this series confirmed that proteasome inhibitor (bortezomib) was toxic to all the cells, but that addition of Hsp90 inhibitor (17-DMAG) could make the compound less effective (**Figure 2.10b**), although this effect was more modest in the PC-3 cells. To explore whether this antagonism might be linked to up-regulation of Hsp72, we performed western blots on the treated lysates. As we observed in the 22Rv1 cells, addition of an Hsp90 inhibitor to the proteasome inhibitor strongly up-regulates Hsp72 at 24 hours in each cell line (**Figure 2.10c**) and the level of elevation was greater than with either compound alone. In addition to these similarities across the four cell lines, we also noted that some relationships depend on the cell type. For example, the combination of Hsp70-Hsp90 inhibitors was only synergistic (ZIP score +2.4) in the 22Rv1 cells (**Figure 2.10a**) and was generally antagonistic in the other cell lines (ZIP score between -4.4 and -4.9). 22Rv1s are the only cell line tested here that expresses both AR and ARv, so this could

be one contributing factor (see **Figure 2.4**). These results highlight the importance of characterizing the wiring of the proteostasis network in each cell line or tumor model.

Discussion

The proteostasis network holds great promise as a source of drug targets for anti-cancer treatment(*37, 38*). However, this concept has met with both successes and failures in the clinic, perhaps requiring a re-examination of the treatment strategies. One logical approach is to use inhibitor combinations, which might limit the ability of cancer proteostasis networks to compensate for loss of one pathway. Although it had been hypothesized that combinations of proteostasis inhibitors might have additivity or even synergy in cancer cells, this possibility had not been systematically quantified. Using a high throughput platform, we revealed clear and reproducible patterns of additivity, synergy and antagonism between inhibitors of four major proteostasis nodes in four different prostate cancer cell lines. We observed that p97 and proteasome inhibitors were especially synergistic in 22Rv1 cells (ZIP score 9.1), a model of castration-resistant prostate cancer (CRPC). Thus, this combination might be used to reduce the dose of both compounds, potentially improving potency while reducing toxicity. In support of this idea, the p97-proteasome inhibitor combination did not produce enhanced cell growth inhibition in non-tumorigenic RWPE-1 cells (see Supplemental Figure 2B). However, it is also important to note that synergy for this combination was not observed in the other three prostate cancer lines, where this combination was modestly antagonistic. Thus, a tailored therapeutic strategy might be required, such as screening primary cells against combinations *ex vivo* to identify synergistic

relationships. Future work will be required to understand whether expression and stability of AR and ARv (see Figure 4A) is predictive of this synergy, as the 22Rv1 cells are the only line tested that expresses both.

We were initially surprised to find drug combinations, exemplified by the Hsp90 and proteasome inhibitor pair, that showed striking antagonism. Within the chosen sub-network (see Figure 1A), we hypothesized that synergy might predominate because of the collaboration between these factors. However, recent studies have introduced the idea of “single-agent dominance” in two-drug combinations(*39*). In this paradigm, molecules that produce a faster onset of cell death can dominate the co-treatment because of cross-talk between cell death pathways. Inhibition of Hsp70, for example, has been shown to induce both apoptosis and necroptosis(*40*), so a deeper exploration of the role of cell death pathways and their kinetics will need to be explored for proteostasis inhibitors and their combinations. Another possibility, potentially supported by our RNA-Seq and western blot findings and not mutually exclusive of “single-agent dominance”, is that the stress responses might be partially responsible for the antagonism of Hsp90 and proteasome inhibitors. Here, the model is that the prostate cancer cells activate this stress signaling program to compensate for loss of function of either Hsp90 or the proteasome. Thus, the combination produces a more robust activation (see Figure 7C) and, accordingly, the potential for increased resistance. Some evidence suggests that this model could be relevant in other cancers. For example, in multiple myeloma cells, treatment with a combinations of Hsp90 and proteasome inhibitors has been suggested to be potentially synergistic based on pre-

clinical studies(*41*) and a clinical trial was conducted in multiple myeloma patients(*42*). However, modest clinical benefit was observed. While there are many possible reasons for this outcome, it is interesting to note that the preclinical studies had shown that the combination strongly increased Hsp70 expression. While our studies were in prostate cancer cells, and not multiple myeloma, it seems possible that this stress response might have limited potency of the combination.

Together, these results suggest that a more comprehensive understanding of which stress pathways are activated by proteostasis inhibitors is likely needed to better track and, ultimately, predict synergy/antagonism, with the goal of designing more effective treatment strategies. One major goal of those efforts could be to profile which stress response pathways are activated by inhibitors to potentially develop predictive biomarkers(*43, 44*). It is starting to become clear that this framework could be more broadly important outside proteostasis targets, as well. For example, treatment with other chemotherapeutics and radiation are capable of eliciting stress responses(*45, 46*), which might likewise blunt their efficacy.

Methods

Cell lines. 22Rv1, LNCaP, C4-2, and PC-3 cells were purchased from ATCC and grown in RPMI 1640 medium supplemented with 10% non heat-inactivated FBS (Gibco 16000044) and 1% penicillin/streptomycin. RWPE-1 cells were purchased from ATCC and grown in K-SFM supplemented with bovine pituitary extract and human recombinant EGF. All cells were grown at 37 °C and 5% CO_2. Cells were regularly

tested for mycobacterial contamination (every 6 months), and maintained at a low passage number.

Inhibitors. JG-98 was prepared, as described(*23*). 17-DMAG was purchased from Cayman Chemical (item #11036). CB-5083 was purchased from Fisher Scientific (catalog #50-115-2549). Bortezomib was purchased from Millipore Sigma (CAS 179324-69-7). AUY-922 was purchased from Fisher Scientific (CAS #747412-49-3). Compounds were used without further purification.

Drug combinations and synergy. All tested compounds were prepared as 10 mM stocks in DMSO and stored in aliquots at -20 °C. For treatments, compounds were then serially diluted in 2-fold increments in RPMI (final DMSO ~ 0.02%). These solutions were then aliquoted to 96-well plates in an 8x8 matrix format for each combination. Concentrations were chosen based on the EC_{50} value of each compound in the cell lines tested, to center the dilution series on the half-maximal value. Specifically, the following final concentrations were used:

Table 2.1. List of compounds and concentration ranges used in proteostasis inhibitor combination screen.

Compound	Concentration range (7 doses, 2 fold dilutions, plus DMSO control)
JG-98	0.16 – 10 μM
17-DMAG	0.016 – 1 μM
CB-5083	0.078 – 5 μM
Bortezomib	0.0015 - 0.1 μM

Cells were grown in tissue-culture treated, 384-well plates (Corning). After 24 hours of cell growth, an Agilent robot was used to transfer compound from the 96-well plates to these 384-well test plates. Cells were returned to 37 °C and 5% CO_2 and grown for three days (doubling time 30-50 hours depending on the cell line). Cell viability was measured using Cell Titer Glo (Promega) according to the manufacturer's instructions and luminescence was measured with a SpectraMax M5 plate reader (Molecular Devices). Cell viability was normalized per plate to the untreated, DMSO control. Synergy was determined using SynergyFinger (http://www.synergyfinderplus.org/). All drug combinations were performed twice per cell line (in technical quadruplicates), and the average mean synergy score for the entire dataset was reported.

Immunoblotting. Cells were plated in 6-well or 12-well plates at 80-100% confluency for 24 hours, after which the medium was replaced with fresh medium containing indicated compounds at 1% DMSO. Compounds were left on cells for the indicated time period (6-24 hours), and cells were incubated at 37 °C and 5% CO_2. Cell lysate was then harvested with M-PER supplemented with protease inhibitor. For measuring phospho-proteins, M-PER was additionally supplemented with phosphatase inhibitor. Lysate was then run on 4-15% gradient SDS polyacrylamide gels at 5-10 µg of total protein per sample. Proteins levels were detected either with Licor florescent secondary antibodies and detected with a Licor machine, or HRP-conjugated secondary antibodies and imaged with BioRad. The following antibodies were used:

Antibodies

The following antibodies and dilutions were used:

Table 2.2: List of antibodies and dilutions used for Western blot studies

Target	Company/Cat #	Dilution used	Host
AR	Abcam (ab133273)	1:2000	Rabbit
BiP	CST (#3177)	1:2000	Rabbit
Hsc70	Enzo (ADI-SPA-816-F)	1:2000	Rabbit
Hsp72	Enzo (ADI-SPA-811-F)	1:2000	Rabbit
Actin	Sigma (A2228)	1:5000	Mouse

RNAseq and Western blot validation

The following concentrations of compounds was used for the RNA-seq studies and subsequent Western blotting:

Table 2.3. List of compounds and concentrations used in RNAseq and Western blot validation studies.

Compound	Concentration
JG-98	0.625 μM
17-DMAG	0.25 μM
CB-5083	0.625 μM
Bortezomib	0.025 μM

Concentrations were chosen based on dose-response and drug synergy landscape data, to best capture combinations of compounds that were either synergistic or antagonistic.

For RNA-seq studies, 22Rv1 cells were plated at 80% confluency in 12-well plates. After 24 hours, cells were dosed with compounds at indicated concentrations and

incubated at 37 °C and 5% CO_2. After 6-hour treatment, RNA was extracted using Zymo Quick-RNA miniprep kit (Catalog #R1054). RNA from all samples were diluted to 20ng/uL in 10 uL for input into TECAN Universal plus mRNA-seq library preparation. RNA-seq libraries were prepared using the manufacture's protocol. RNA-seq libraries were sequenced for quality control on an Illumina MiniSeq and pooled according to protein coding read counts to obtain uniform protein coding read depth. The final pools were sequenced using single end 50bp reads on an Illumina HiSeq 4000 at the Center for Advanced Technology (www.cat.ucsf.edu). Sequencing reads were aligned to the Human reference genome (Build HG38) and the Ensembl gene annotation (version 95) using STAR (v2.7.2b; PMID: 23104886). Read counts per gene as output by STAR were collapsed into a read counts matrix and were used as input to DESeq2 (v1.24.0; PMID: 25516281) to test for differential gene expression between conditions using a Wald test. Genes passing a multiple testing correct p-value of 0.1 (FDR method) were considered significant.

For western blot validation of RNA-seq, 22Rv1 cells were plated and dosed at the same conditions. Following drug-treatment, immunoblotting was performed as described above.

Figures

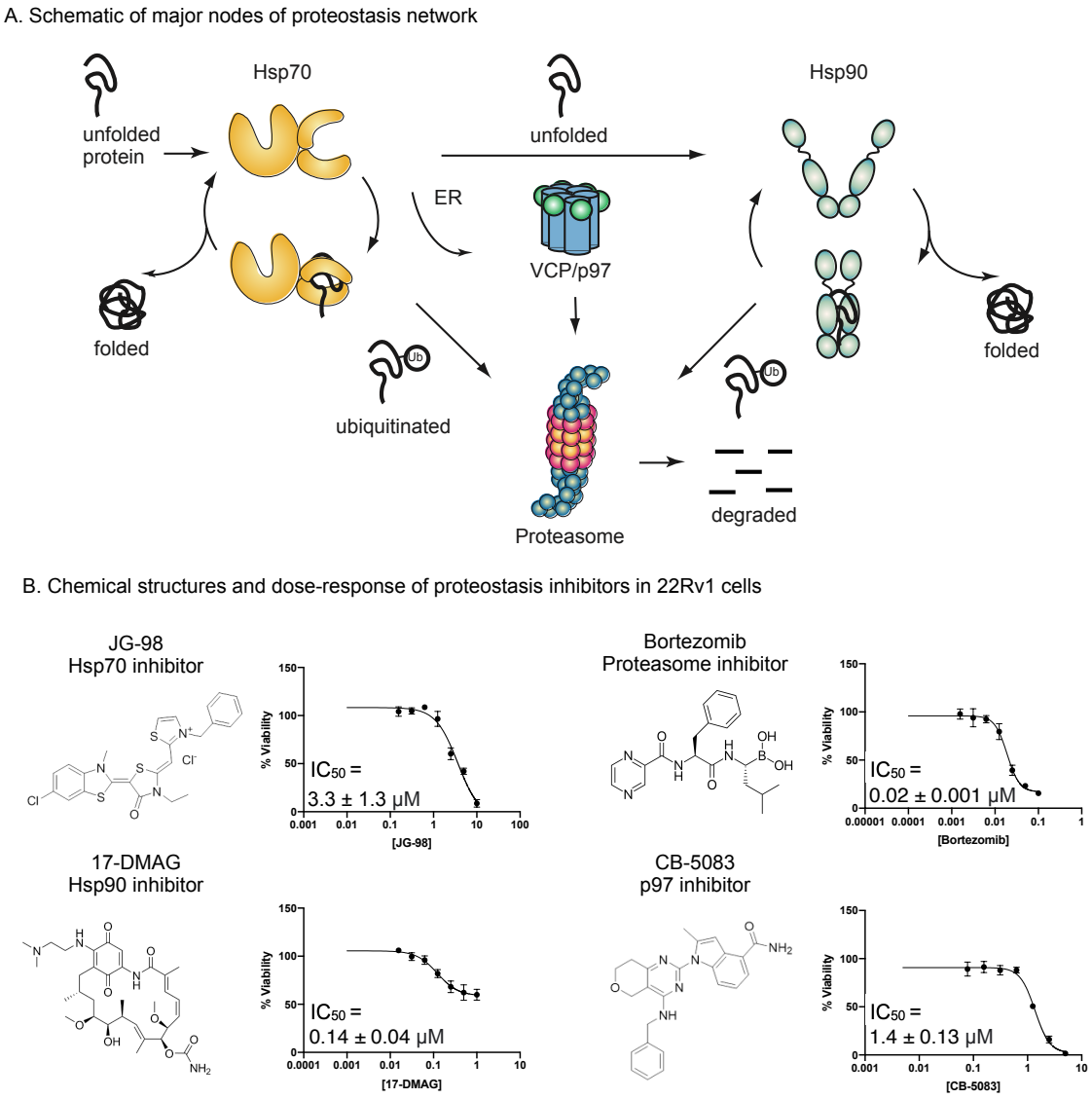

Figure 2.1. Proteostasis inhibitors, targeting multiple nodes of the proteostasis network, have anti-proliferative effects in 22Rv1 prostate cancer cells. A. A subset of the proteostasis network is shown, highlighting the connections between the major nodes: Hsp70, Hsp90, p97, and the proteasome. Together, these factors guide protein folding and turnover, working together to mediate client "hand-off". B. Inhibitors of proteostasis nodes limit growth of 22Rv1 cells. In this study, four inhibitors were used: JG-98 (Hsp70 inhibitor), 17-DMAG (Hsp90 inhibitor), bortezomib (proteasome inhibitor) and CB-5083 (p97 inhibitor). Cells were incubated with the indicated compound for 72 hours, and viability measured via Cell Titer Glo (see Methods). Results are the average of experiments performed in quadruplicate and the error bars represent SD. Some error bars are smaller than symbols.

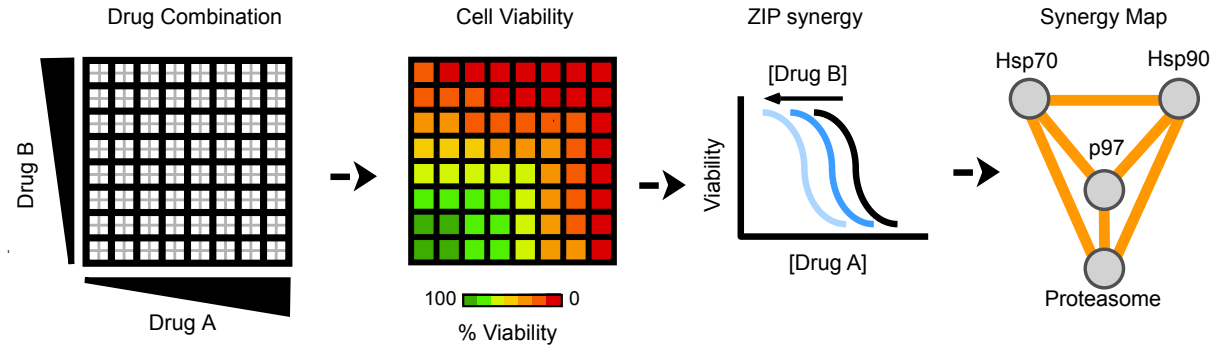

Figure 2.2. Workflow for the measurement of additivity, synergy or antagonism amongst proteostasis inhibitors. Briefly, cells are aliquoted to 384-well plates and allowed to adhere for one day. Then, two drugs (A and B) are added in an 8x8 matrix format, with 7 doses per compound, using 2-fold dilutions (see Methods for tested concentrations) and a DMSO solvent control. Treatments were performed in quadruplicate, with 4 wells per each dose combination (grey squares). After 72-hours of treatment, cell viability was measured using Cell Titer Glo, and synergy determined through the ZIP synergy model. Drug-combination screens were performed twice per cell line, and ZIP synergy score was averaged between replicates. Under this model, addition of Drug B reducing the potency of Drug A (blue lines) would be considered synergy. ZIP scores around zero (between 1.5 and -1.5) were considered additive, while scores above 1.5 were considered synergistic and those below -1.5 were considered antagonistic. To map these relationships onto the proteostasis subnetwork (see Fig 1A), we plotted the nodes and created lines between them to indicate whether the ZIP synergy score was additive, synergistic or antagonistic for each tested cell line (termed a Synergy Map).

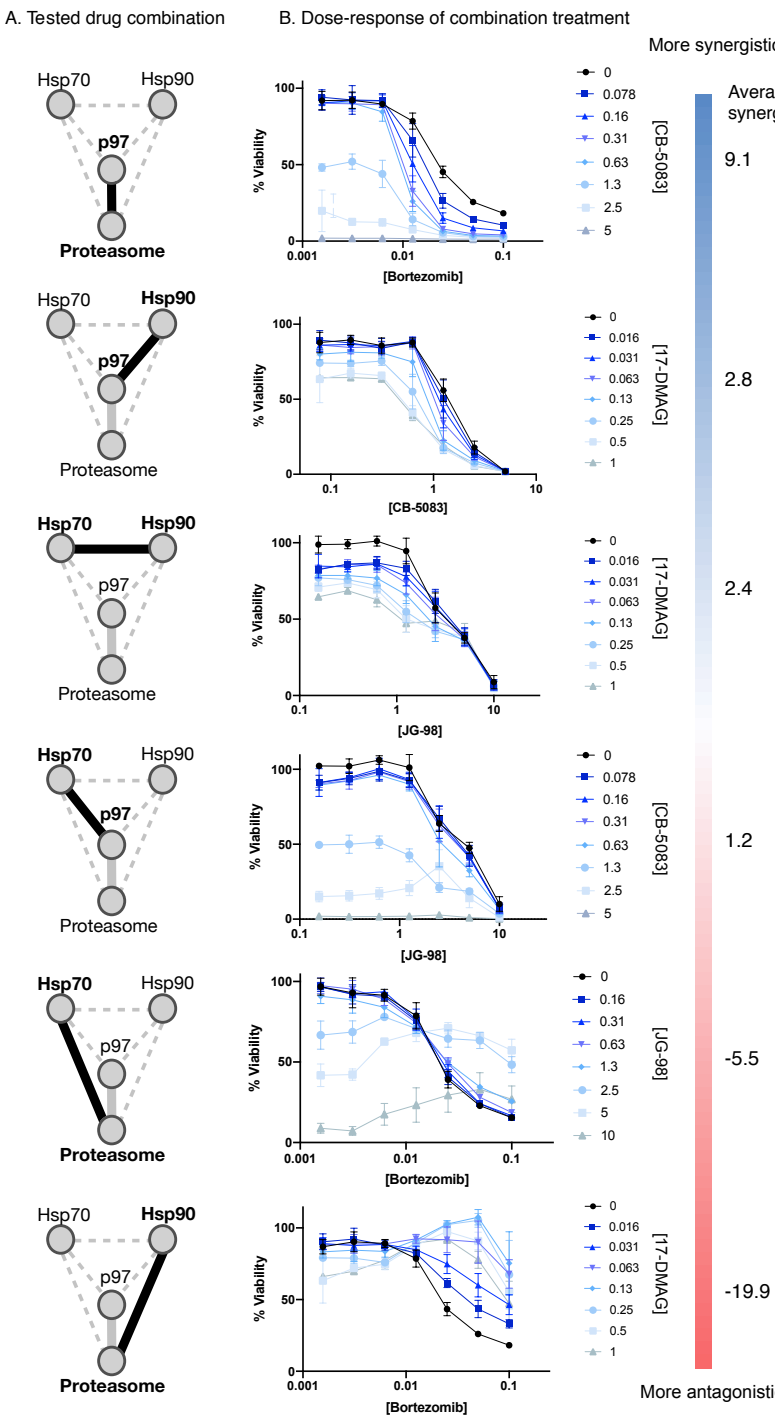

Figure 2.3. Combinations were either additive, synergistic or antagonistic in 22Rv1 cells. A. For each combination, a black line and bolded text indicates the tested nodes on the Synergy Map in the highlighted adjacent dose-response panel. B. Dose-response curves from each combination are used to highlight additivity, synergy or antagonism. In each graph, the single-agent (black) and combination treatments (blue curves) are shown. Curves are arranged from top to bottom from the most synergistic to the most antagonistic, with the average ZIP synergy scores shown. For the full matrix landscape of the cell viability and synergy results, see Figure 2.4.

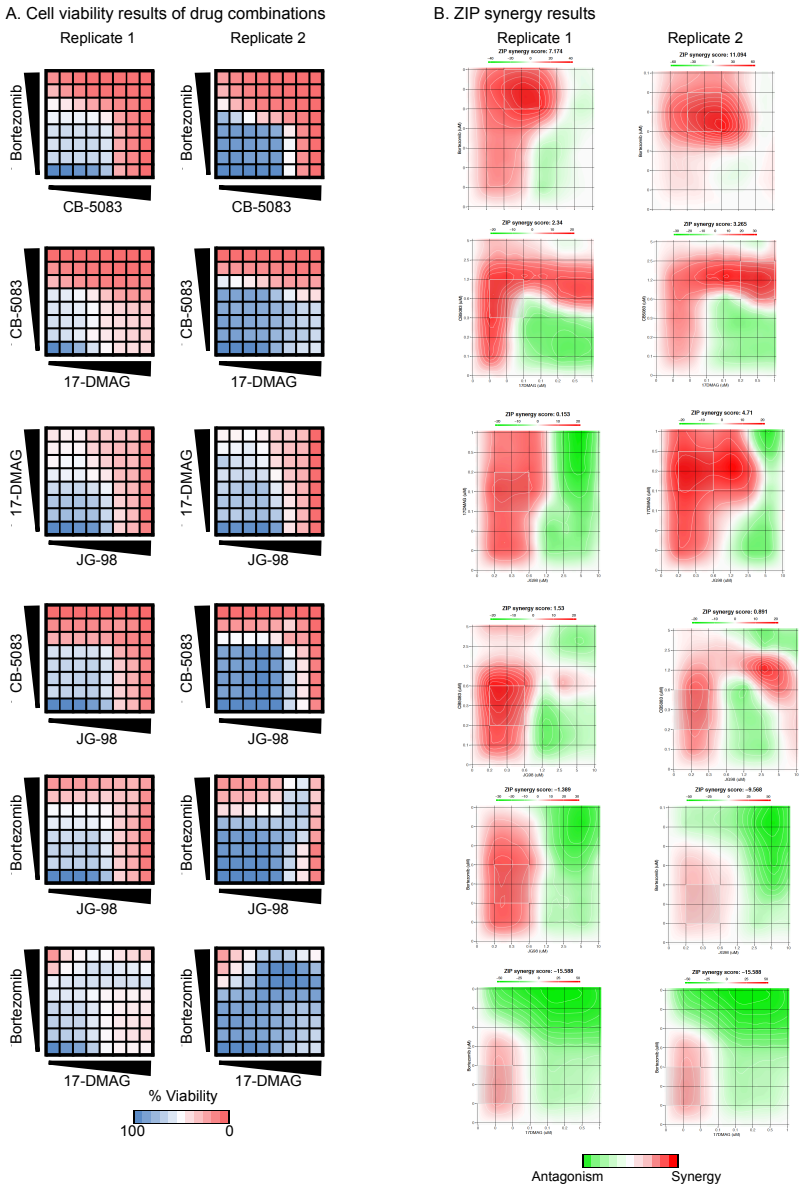

Figure 2.4. Strong reproducibility was observed in 22Rv1 cells treated with proteostasis inhibitor combinations. A. Cell viability results of 22Rv1 treated with indicated proteostasis inhibitor combinations. Viability was measured via Cell Titer Glo following 72 hours of compound treatment, performed in quadruplicate (see Methods). Viability results are reproducible between replicates, and vary depending on the combination of compounds. B. ZIP synergy output of the proteostasis inhibitor combinations. High reproducibility is observed between replicates, with similar patterns of synergy and antagonism across the plate landscape.

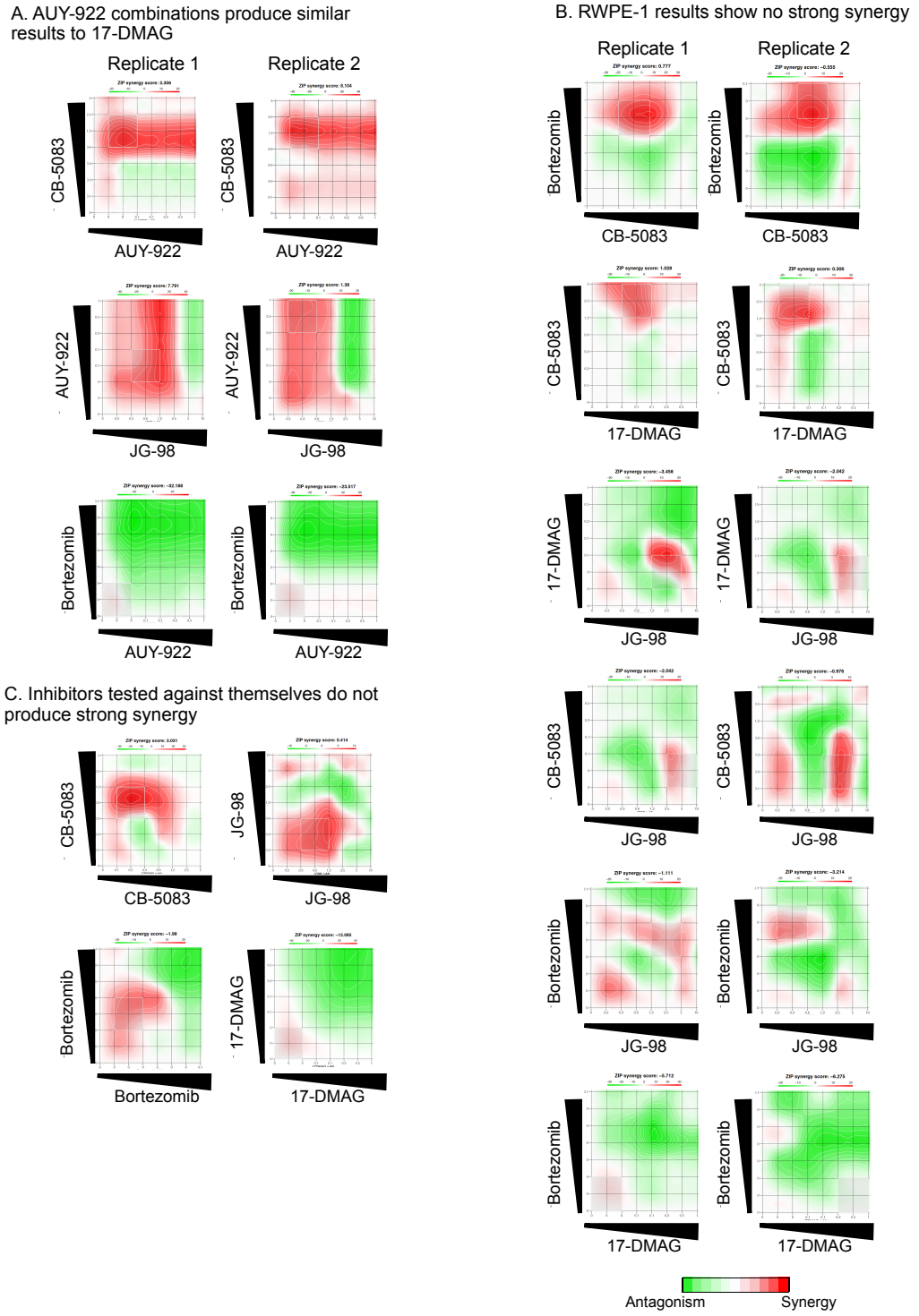

Figure 2.5. Various control studies were performed with the proteostasis inhibitors A. AUY-922, an alternative Hsp90 inhibitor, was tested in combination with the other proteostasis inhibitors, and produced similar results to 17-DMAG. B. Inhibitor combinations were tested in RWPE-1 cells, a non-tumorigenic prostate cell line, and did not produce any strong synergies. C. Each inhibitor was tested against itself and did not produce strong synergy across the tested landscape.

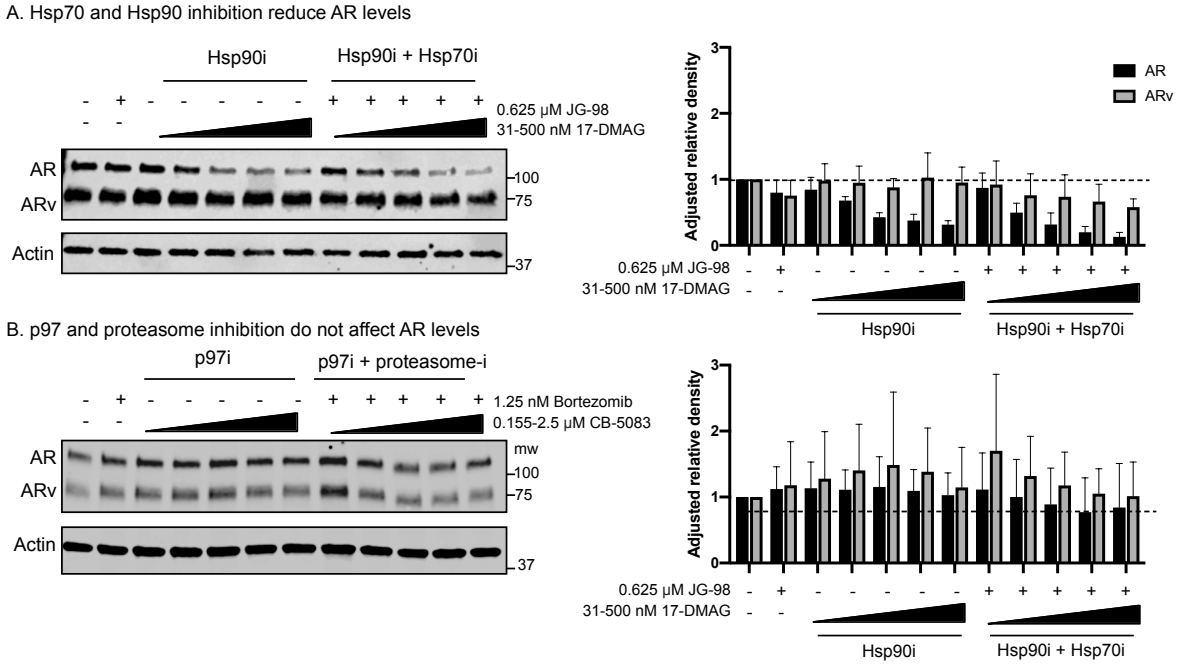

Figure 2.6. Some combinations reduce androgen receptor levels, but others do not. Effects of proteostasis inhibitor combinations on AR levels in 22Rv1 cells following 6-hour treatment. A. Treatment with the Hsp90 inhibitor 17-DMAG reduces the levels of full length AR, and Hsp70 inhibitor JG-98 treatment reduces levels of both AR and ARv in 22Rv1 cells after 6 hours. The combination was effective at reducing both proteins. B. Neither the p97 nor proteasome inhibitor, or their combination, had an effect on AR or ARv levels at 6 hours. Western blots are representative of experiments performed in triplicate. The blots were quantified in NIH Image J and the average density adjusted to the loading control and DMSO treatment was plotted on the right. Error bars represent SD.

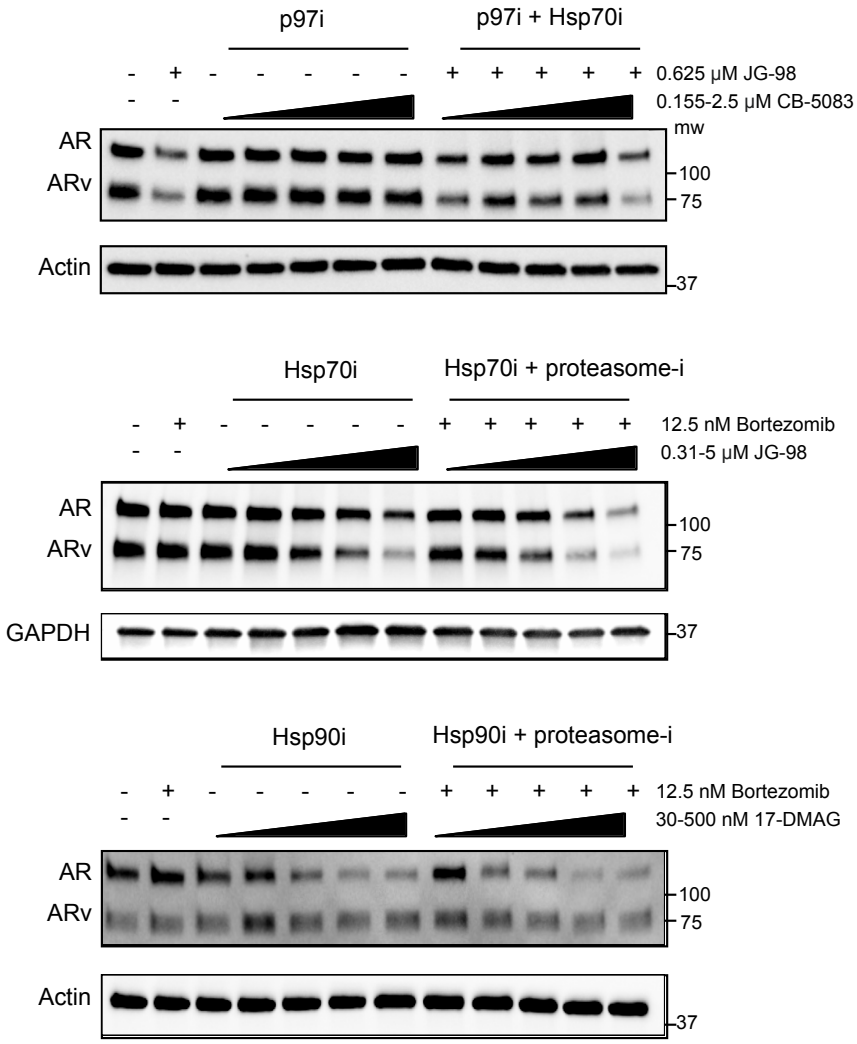

Figure 2.7. Effects of additional proteostasis inhibitor combinations on AR levels in 22Rv1 cells. Three additional inhibitor combinations were tested, p97-Hsp70, Hsp70-proteasome, and Hsp90-proteasome. No observable differences were seen between single-agent treatment and combinations. Western blots are representative of experiments performed in duplicate.

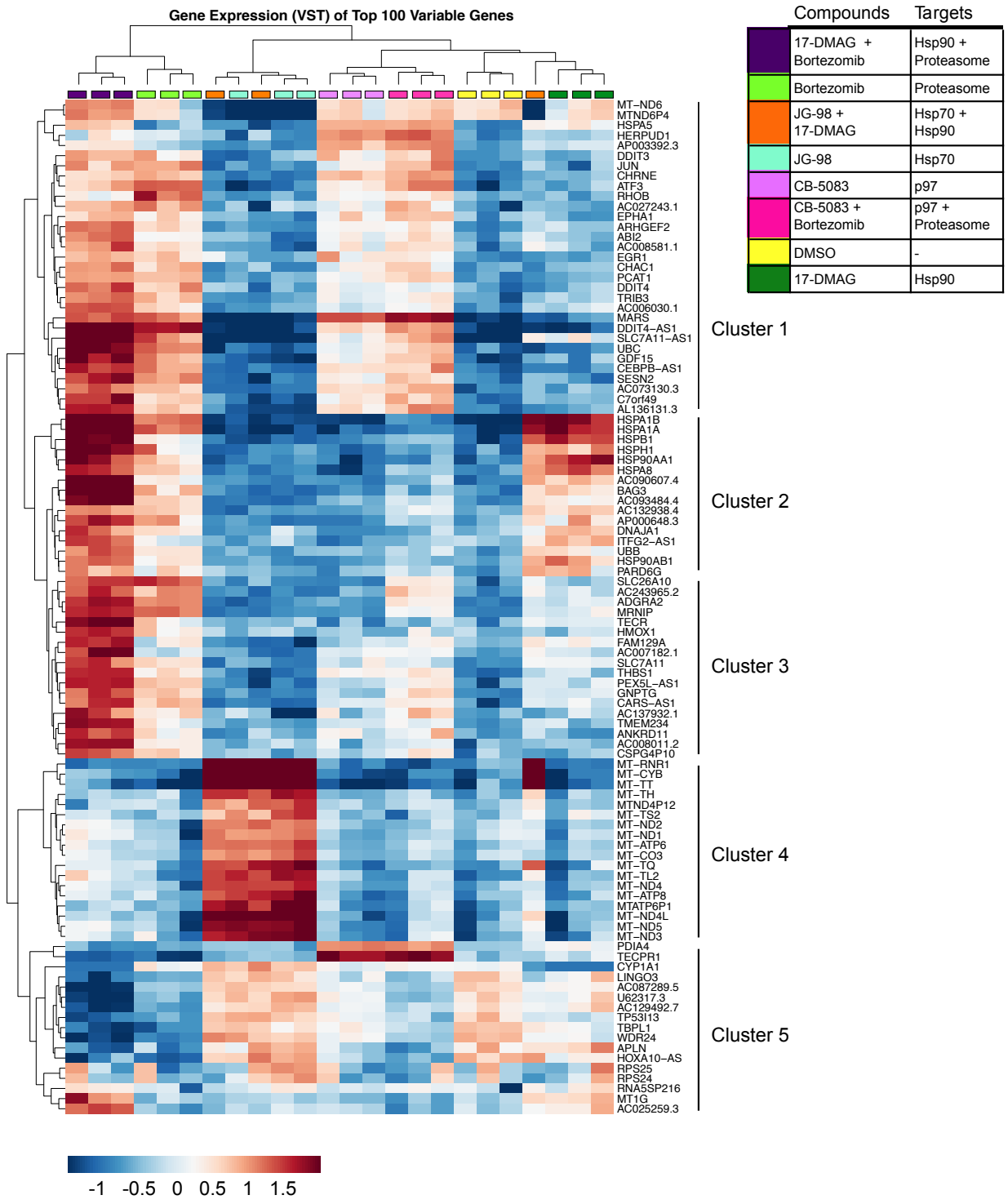

Figure 2.8. RNA-seq data highlights differences in gene expression following single-agent and combination proteostasis inhibitor treatment. 22Rv1 cells were treated with indicated compounds for 6 hours, after which RNA-seq was performed. The top 100 variably expressed genes across all conditions were clustered and further analyzed.

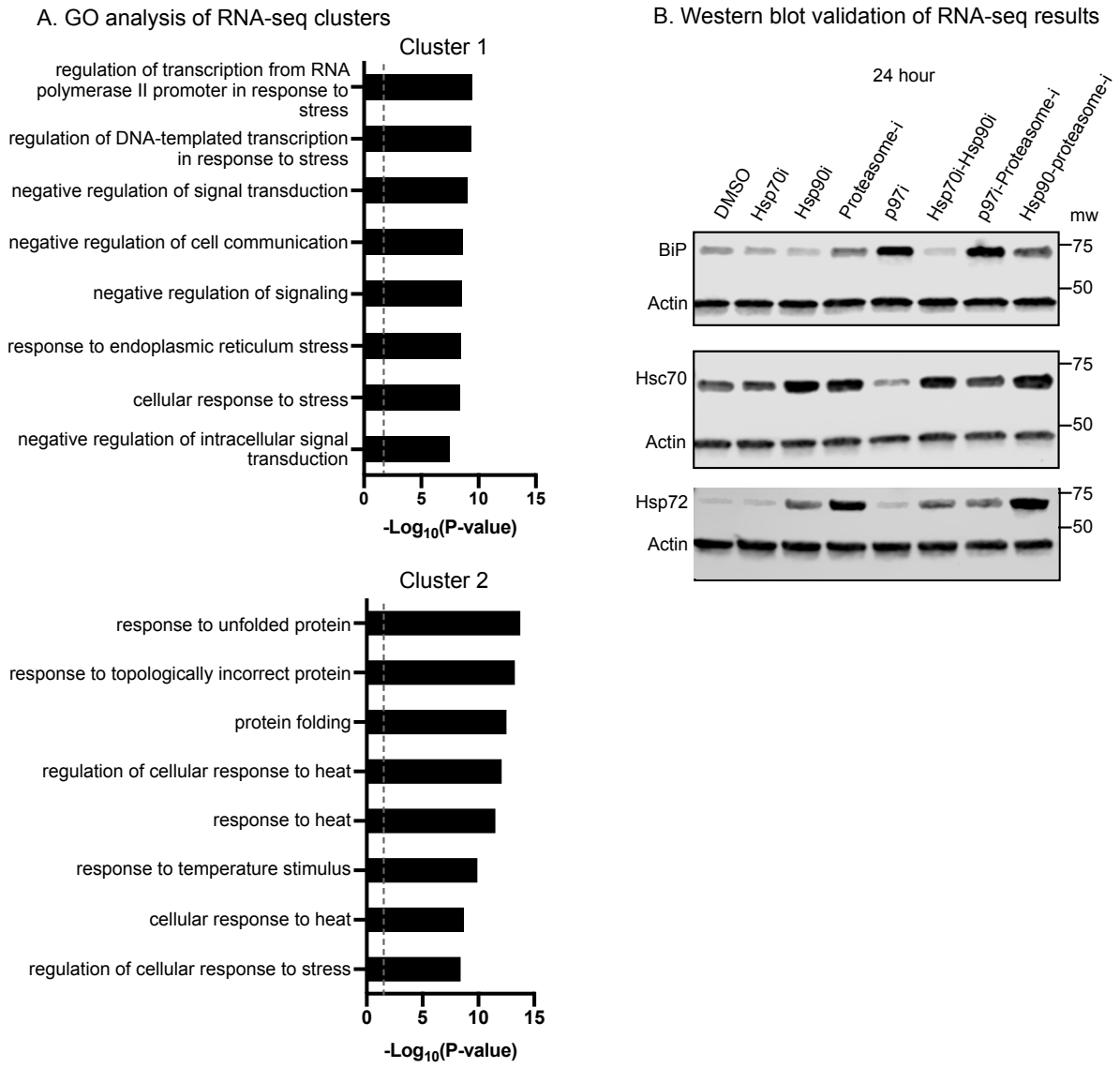

Figure 2.9. RNA-seq studies and protein level validation highlight differences in activation of stress response pathways between single-agent and combination proteostasis inhibitor treatments. A. Gene ontology (GO) analysis of clusters 1 and 2 from top variably expressed genes (see Figure 2.8). Top 8 most significantly enriched GO terms are shown. B. BiP, Hsc70, and Hsp72 levels were probed via Western blot following 24 hours of compound treatment (see Methods for concentrations used). Protein levels at 24 hours closely match transcriptomic data and are differentially expressed across single-agent and combination proteostasis inhibition. Results are representative of experiments performed in triplicate.

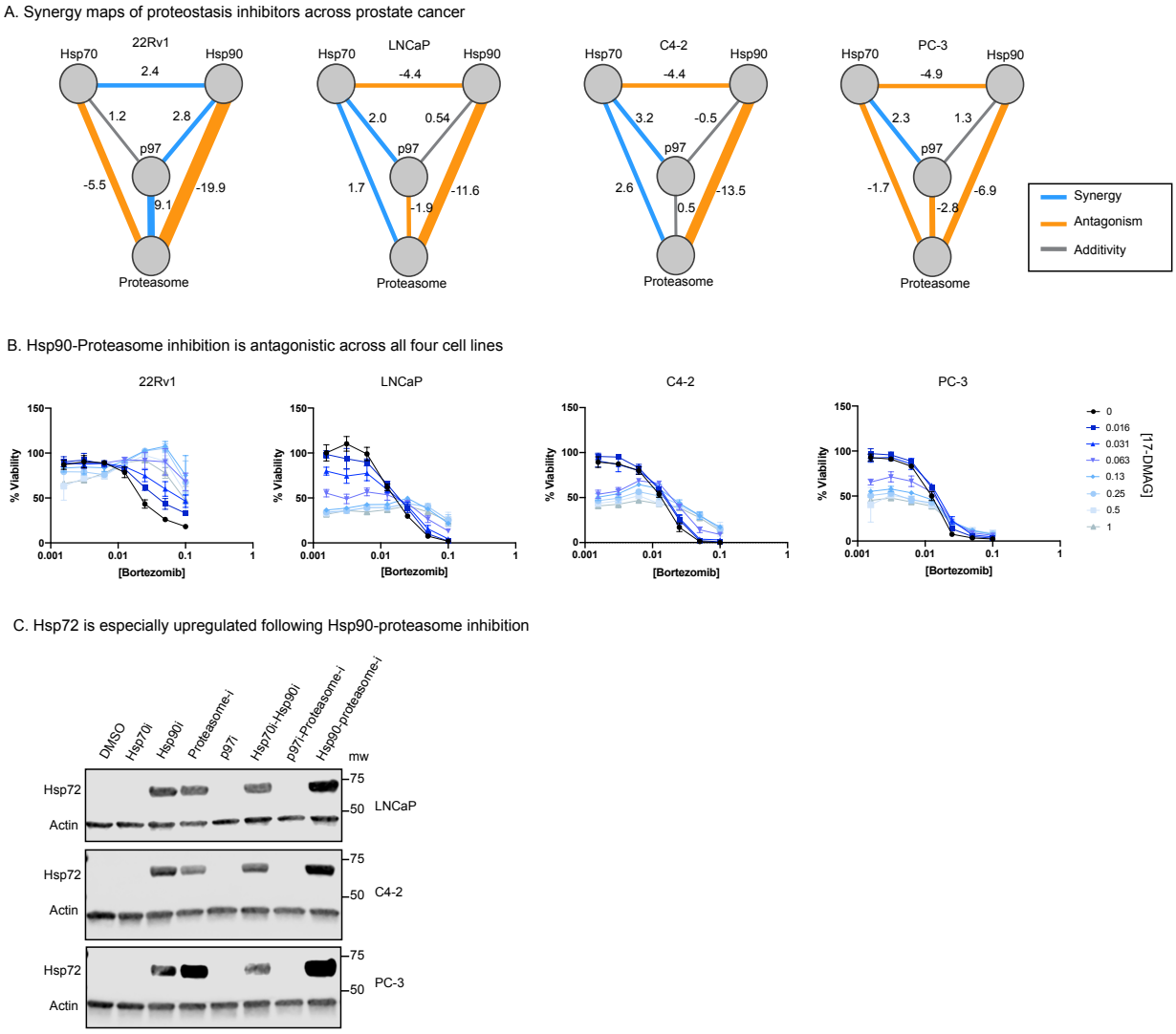

Figure 2.10. Expanded screens in additional prostate cancer cell lines reveals both similarities and differences in their responses to combinations of proteostasis inhibitor treatment. A. Synergy maps depicting the relationship between proteostasis nodes from the drug-combination screens. Synergy is blue, antagonism is orange, and additivity is gray. Cutoffs defined in Figure 2.2 were applied here. Screens were performed as described in Figure 2.2, with each dose-combination performed in quadruplicate. Each screen was performed twice per cell line, and synergy scores were averaged. B. Representative dose-response curves from the antagonistic combination of proteasome-Hsp90 inhibitors. In each example, the proteasome inhibitor (bortezomib) alone is shown in black, while the combinations with the Hsp90 inhibitor 17-DMAG are shown with blue lines. Results are the average of quadruplicate and error bars are SD. Some error bars are smaller than the symbols. C. Hsp72 is upregulated following Hsp90 and proteasome inhibition in all of the cell lines tested, by Western blot. Results are representative of experiments performed in triplicate.

References

1. S. Sannino *et al.*, Compensatory increases of select proteostasis networks after Hsp70 inhibition in cancer cells. *J Cell Sci* **131**, (2018).
2. P. Workman, F. Burrows, L. Neckers, N. Rosen, Drugging the cancer chaperone HSP90: combinatorial therapeutic exploitation of oncogene addiction and tumor stress. *Ann N Y Acad Sci* **1113**, 202-216 (2007).
3. K. Zhu, K. Dunner, Jr., D. J. McConkey, Proteasome inhibitors activate autophagy as a cytoprotective response in human prostate cancer cells. *Oncogene* **29**, 451-462 (2010).
4. D. J. Anderson *et al.*, Targeting the AAA ATPase p97 as an Approach to Treat Cancer through Disruption of Protein Homeostasis. *Cancer cell* **28**, 653-665 (2015).
5. S. Sannino *et al.*, Unique integrated stress response sensors regulate cancer cell susceptibility when Hsp70 activity is compromised. *eLife* **10**, (2021).
6. S. P. Shah *et al.*, Bortezomib-induced heat shock response protects multiple myeloma cells and is activated by heat shock factor 1 serine 326 phosphorylation. *Oncotarget* **7**, 59727-59741 (2016).
7. Y. Bai, X. Su, Updates to the drug-resistant mechanism of proteasome inhibitors in multiple myeloma. *Asia Pac J Clin Oncol* **17**, 29-35 (2021).
8. M. V. Powers, P. A. Clarke, P. Workman, Dual targeting of HSC70 and HSP72 inhibits HSP90 function and induces tumor-specific apoptosis. *Cancer cell* **14**, 250-262 (2008).

9. M. Shevtsov *et al.*, Combination of Anti-Cancer Drugs with Molecular Chaperone Inhibitors. *International journal of molecular sciences* **20**, (2019).

10. A. I. P. Eugenio *et al.*, Proteasome and heat shock protein 70 (HSP70) inhibitors as therapeutic alternative in multiple myeloma. *Oncotarget* **8**, 114698-114709 (2017).

11. A. Cavanaugh, B. Juengst, K. Sheridan, J. F. Danella, H. Williams, Combined inhibition of heat shock proteins 90 and 70 leads to simultaneous degradation of the oncogenic signaling proteins involved in muscle invasive bladder cancer. *Oncotarget* **6**, 39821-39838 (2015).

12. M. A. Moses *et al.*, Targeting the Hsp40/Hsp70 chaperone axis as a novel strategy to treat castration-resistant prostate cancer. *Cancer Res*, (2018).

13. P. C. Echeverria, D. Picard, Molecular chaperones, essential partners of steroid hormone receptors for activity and mobility. *Biochim Biophys Acta* **1803**, 641-649 (2010).

14. F. U. Hartl, M. Hayer-Hartl, Converging concepts of protein folding in vitro and in vivo. *Nat Struct Mol Biol* **16**, 574-581 (2009).

15. P. H. Vekaria, T. Home, S. Weir, F. J. Schoenen, R. Rao, Targeting p97 to Disrupt Protein Homeostasis in Cancer. *Front Oncol* **6**, 181 (2016).

16. G. A. Collins, A. L. Goldberg, The Logic of the 26S Proteasome. *Cell* **169**, 792-806 (2017).

17. B. D. Johnson, R. J. Schumacher, E. D. Ross, D. O. Toft, Hop modulates Hsp70/Hsp90 interactions in protein folding. *J Biol Chem* **273**, 3679-3686 (1998).

18. E. Kirschke, D. Goswami, D. Southworth, P. R. Griffin, D. A. Agard, Glucocorticoid receptor function regulated by coordinated action of the Hsp90 and Hsp70 chaperone cycles. *Cell* **157**, 1685-1697 (2014).

19. M. K. Lemberg, K. Strisovsky, Maintenance of organellar protein homeostasis by ER-associated degradation and related mechanisms. *Mol Cell* **81**, 2507-2519 (2021).

20. J. L. Brodsky, The protective and destructive roles played by molecular chaperones during ERAD (endoplasmic-reticulum-associated degradation). *Biochem J* **404**, 353-363 (2007).

21. L. Petrucelli *et al.*, CHIP and Hsp70 regulate tau ubiquitination, degradation and aggregation. *Hum Mol Genet* **13**, 703-714 (2004).

22. C. A. Dickey *et al.*, The high-affinity HSP90-CHIP complex recognizes and selectively degrades phosphorylated tau client proteins. *J Clin Invest* **117**, 648-658 (2007).

23. X. Li *et al.*, Analogs of the Allosteric Heat Shock Protein 70 (Hsp70) Inhibitor, MKT-077, as Anti-Cancer Agents. *ACS medicinal chemistry letters* **4**, 1042-1047 (2013).

24. M. P. Goetz, D. O. Toft, M. M. Ames, C. Erlichman, The Hsp90 chaperone complex as a novel target for cancer therapy. *Annals of oncology : official journal of the European Society for Medical Oncology / ESMO* **14**, 1169-1176 (2003).

25. R. Arkwright, T. M. Pham, J. A. Zonder, Q. P. Dou, The preclinical discovery and development of bortezomib for the treatment of mantle cell lymphoma. *Expert Opin Drug Discov* **12**, 225-235 (2017).

26. S. C. Kaul, C. C. Deocaris, R. Wadhwa, Three faces of mortalin: A housekeeper, guardian and killer. *Exp Gerontol* **42**, 263-274 (2007).

27. B. Yadav, K. Wennerberg, T. Aittokallio, J. Tang, Searching for Drug Synergy in Complex Dose-Response Landscapes Using an Interaction Potency Model. *Comput Struct Biotechnol J* **13**, 504-513 (2015).

28. R. J. Tallarida, Quantitative methods for assessing drug synergism. *Genes Cancer* **2**, 1003-1008 (2011).

29. T. C. Chou, P. Talalay, Quantitative analysis of dose-effect relationships: the combined effects of multiple drugs or enzyme inhibitors. *Adv Enzyme Regul* **22**, 27-55 (1984).

30. C. T. Meyer, D. J. Wooten, C. F. Lopez, V. Quaranta, Charting the Fragmented Landscape of Drug Synergy. *Trends in pharmacological sciences* **41**, 266-280 (2020).

31. A. H. C. Vlot, N. Aniceto, M. P. Menden, G. Ulrich-Merzenich, A. Bender, Applying synergy metrics to combination screening data: agreements, disagreements and pitfalls. *Drug discovery today* **24**, 2286-2298 (2019).

32. Q. Feng, B. He, Androgen Receptor Signaling in the Development of Castration-Resistant Prostate Cancer. *Front Oncol* **9**, 858 (2019).

33. P. A. Watson, V. K. Arora, C. L. Sawyers, Emerging mechanisms of resistance to androgen receptor inhibitors in prostate cancer. *Nature reviews* **15**, 701-711 (2015).

34. B. Eftekharzadeh *et al.*, Hsp70 and Hsp40 inhibit an inter-domain interaction necessary for transcriptional activity in the androgen receptor. *Nature communications* **10**, 3562 (2019).

35. J. Anckar, L. Sistonen, Regulation of HSF1 Function in the Heat Stress Response: Implications in Aging and Disease. *Annu Rev Biochem*, (2011).

36. R. Wadhwa *et al.*, Selective toxicity of MKT-077 to cancer cells is mediated by its binding to the hsp70 family protein mot-2 and reactivation of p53 function. *Cancer Res* **60**, 6818-6821 (2000).

37. S. Joshi *et al.*, Adapting to stress - chaperome networks in cancer. *Nature reviews* **18**, 562-575 (2018).

38. S. Sannino, J. L. Brodsky, Targeting protein quality control pathways in breast cancer. *BMC Biol* **15**, 109 (2017).

39. R. Richards *et al.*, Drug antagonism and single-agent dominance result from differences in death kinetics. *Nat Chem Biol* **16**, 791-800 (2020).

40. S. R. Srinivasan *et al.*, Heat Shock Protein 70 (Hsp70) Suppresses RIP1-Dependent Apoptotic and Necroptotic Cascades. *Molecular cancer research : MCR* **16**, 58-68 (2018).

41. T. Ishii *et al.*, Anti-tumor activity against multiple myeloma by combination of KW-2478, an Hsp90 inhibitor, with bortezomib. *Blood cancer journal* **2**, e68 (2012).

42. J. Cavenagh *et al.*, A phase I/II study of KW-2478, an Hsp90 inhibitor, in combination with bortezomib in patients with relapsed/refractory multiple myeloma. *Br J Cancer* **117**, 1295-1302 (2017).

43. K. Dhama *et al.*, Biomarkers in Stress Related Diseases/Disorders: Diagnostic, Prognostic, and Therapeutic Values. *Frontiers in molecular biosciences* **6**, 91 (2019).

44. R. Bagatell *et al.*, Induction of a heat shock factor 1-dependent stress response alters the cytotoxic activity of hsp90-binding agents. *Clin Cancer Res* **6**, 3312-3318 (2000).

45. E. Tiligada, Chemotherapy: induction of stress responses. *Endocrine-related cancer* **13 Suppl 1**, S115-124 (2006).

46. W. Kim *et al.*, Cellular Stress Responses in Radiotherapy. *Cells* **8**, (2019).

Chapter 3:

Genetic perturbations reveal selective vulnerabilities in the proteostasis network of Castration-Resistant Prostate Cancer (CRPC)

Abstract

Castration-resistant prostate cancer (CRPC) is associated with an increased reliance on protein homeostasis (aka proteostasis) factors, such as heat shock protein 70 (Hsp70), but it is not clear what other factors might be involved. To address this question, we performed functional and synthetic lethal screens in four prostate cancer cell lines. These screens confirmed key roles for Hsp70, Hsp90 and their co-chaperones, but also suggested that the mitochondrial chaperone, Hsp60/HSPD1 is selectively required in CRPC cell lines. Knockdown of Hsp60 did not impact the stability of androgen receptor (AR) or its variants; rather, it was associated with loss of mitochondrial spare respiratory capacity, partly due to increased proton leakage. Finally, transcriptional data revealed a correlation between Hsp60 levels and poor survival of prostate cancer patients. These findings suggest that re-wiring of the proteostasis network is associated with CRPC, creating selective vulnerabilities that might be targeted to treat the disease.

Introduction

Protein homeostasis (proteostasis) is achieved when the overall rates of protein folding, trafficking, and degradation are balanced (*1*). This balance is maintained by the proteostasis network, a collection of interconnected pathways, which include molecular chaperones, stress response signaling factors and protein quality control systems. In cancer cells, unique demands are placed on the proteostasis network, owing to their rapid growth rates, unusual metabolic requirements, and high mutational loads (*2-5*). This dependence has been described as a “non-oncogene addiction” (*6, 7*) and individual components of the proteostasis network have been pursued as attractive anti-

cancer targets. In the clinic, such attempts have yielded both dramatic successes and confounding failures (*8*). One potential reason for this uneven level of success is that the field is only beginning to probe how proteostasis networks are functionally different in cancer cells vs. normal cells or between different stages of cancer (*9-12*).

Prostate cancer (PCa) is an especially interesting system for probing these questions. PCa cells typically rely on transcriptional programs driven by the androgen receptor (AR), and many prostate tumors therefore initially respond well to androgen depravation therapy (ADT). However, following ADT, the disease invariably progresses to castration-resistant prostate cancer (CRPC) (*13-15*). In CRPC cells, AR activity is usually able to persist through amplification, mutations, and constituitively-active splice variants of AR (ARv) (*16-20*) and compensation by other steroid hormone receptors (SHRs), such as the glucocorticoid receptor (*21, 22*). Additionally, the conversion from PCa to CRPC is associated with metabolic reprogramming (*23*). Thus, it seems likely that, to account for these molecular and metabolic changes, the proteostasis networks of PCa and CRPC cells might need to be distinct. For example, like other SHRs, AR is known to require an elaborate set of chaperones, including heat shock protein 70 (Hsp70), heat shock protein 90 (Hsp90) and their co-chaperones, for its folding, activation and degradation (*24-27*). Accordingly, chemical inhibitors of Hsp90 are known to promote degradation of AR in PCa cells (*28*) and these inhibitors show synergy with ADT (*29*). Similar findings have been observed when targeting essential Hsp90 co-chaperones (*30*). However, Hsp90 inhibitors are less effective in cellular models of CRPC, such as 22Rv1, which are driven by ARv signaling. Instead, inhibitors of Hsp70 have been shown to decrease

the stability of ARvs and have anti-proliferative activity in these cells (*28*). This difference in chaperone inhibitor sensitivity between PCa and CRPC cells might be partially explained by molecular differences in recognition of AR and its variants. Specifically, Hsp70, but not Hsp90, binds to the N-terminal motif that remains in the ARv found in 22Rv1 cells (*31, 32*). Thus, CRPC is an interesting model for studying the role of proteostasis networks, given the reliance of these cells on Hsp70, Hsp90, AR and its variants.

While there is growing evidence for the roles of Hsp70 and Hsp90 in PCa and CRPC, it is not yet clear whether the broader proteostasis network might be "re-wired" to accommodate the demands of CRPC. Here, we used functional genomics screening to identify selective vulnerabilities in PCa and CRPC cell lines. In that effort, we deployed a focused shRNA collection, termed the Proteostasis Library (*33*), that allows knockdown of ~140 molecular chaperones, co-chaperones and related factors. In addition, we searched for synthetic lethality by repeating the screens in the presence of chemical inhibitors of Hsp70 and Hsp90. The results identified factors that are required in all of the cells (*e.g.* shared vulnerabilities), but also ones that are unique to PCa or CRPC cell lines. One of the most striking findings was that the mitochondrial chaperone, Hsp60 (gene name HSPD1) is required for growth of CRPC cells, but not PCa cells. Knockdown studies suggest that, unlike Hsp70 and Hsp90, this chaperone is not involved in AR or ARv stability; rather, decreases in Hsp60 levels in 22Rv1 cells were associated with loss of mitochondrial spare respiratory capacity. The relationship between Hsp60 and CRPC was further validated by analysis of transcriptional data from

PCa and ADT-treated patient samples, which showed a strong correlation between Hsp60 transcript levels and poor disease outcomes. Together, these results identify a potential drug target for the treatment of CRPC, as well as more broadly suggesting how proteostasis networks are adapted to provide drug resistance in prostate cancer.

Results:

Design of the Proteostasis Library. To explore the chaperone dependences of PCa and CRPC cell lines, we used a focused shRNA library, termed the Proteostasis Library, that targets 139 genes encoding chaperones and related factors (**Figure 3.1a**). This library is composed of 25 targeting sequences per gene, plus an additional 500 control, non-targeting sequences. These shRNA sequences are cloned into a lentiviral vector and used in a pooled screen format, as previously described (*33*-*35*). The genes selected for inclusion in this library include examples of the major chaperone families, such as Hsp70s, Hsp90s, chaperonins (TRiC/CCT) and small heat shock proteins (sHsps) (**Figure 3.1a**). It also includes the major co-chaperones for Hsp70s, such as J-domain proteins (JDPs, also called Hsp40s), tetratricopeptide repeat (TPR) domain proteins and nucleotide-exchange factors (NEFs), and the major co-chaperones for Hsp90, such as CDC37, AHA1 and PTGE53 (also called p23). Beyond chaperones and co-chaperones, the library includes other protein folding and maintenance enzymes, such as protein disulfide isomerases (PDIs), peptidyl prolyl isomerases (PPIases), and factors required for proteasome assembly (*e.g.* PSMG1) and protein trafficking (*e.g.* VCP/97, Sec63). Finally, the library covers a subset of targets that are involved in stress signaling pathways, including HSF1/2, ATF6 and XBP1. It is worth noting that, although

CRISPR/Cas9-based methods are also a powerful, alternative way to perform screens, we favored the shRNA approach in this case because it can be used in multiple cell lines without the requirement for stable expression of Cas9/dCas9. Together, this shRNA library provides broad coverage of the major functional and regulatory components of the proteostasis network, allowing potential identification of cancer sensitivities across various functions.

In assembling the Proteostasis Library, we favored groups of targets that are known to physically bind to each other (bold and dotted lines in **Figure 3.1a**). One of the defining features of the proteostasis network is that many of the components engage in protein-protein interactions (PPIs), both with each other and with their client proteins (*36*). Another feature of this network is that there is potential redundancy built into it. For example, in human cells there are genes for ~13 Hsp70s, ~50 JDPs, and 6 Hsp90s (*37-39*). To illustrate this design feature in Figure 2.1a, we clustered the genes in functional families and depict them as a schematic map that highlights the PPIs. For each class, there are members that are localized to specific sub-cellular locations; for example, the major Hsp70s of the cytosol are Hsp72 (HSP1A1) and Hsc70 (HSPA8), while BiP/HSPA5 and mortalin/HSPA9 are found in the ER and mitochondria, respectively (*40*).

Functional genomics screen to identify shared and unique vulnerabilities in PCa and CRPC cell lines. Using the Proteostasis Library, we conducted a functional genomics screen by transducing cells with the pooled shRNAs, growing them for 10

doubling times, and then deep sequencing at the initial (T_0) and final (T_{final}) time points (**Figure 3.1b**). Results on the individual shRNA level showed that the screens produced viable results and the negative controls behaved as expected (**Figure 3.2**). From these results, we determined the phenotype and p-value of each gene knockdown,as described (*35*). Here, phenotype is calculated by comparing the shRNA frequencies at the T_0 and T_{final} time points, along with the cell growth rate, and the Mann-Whitney P-value is calculated by comparing the results of the 25 shRNAs per gene to the negative control shRNAs.

These screens were conducted in four different cell lines. Two of these lines (22Rv1 and C-42) are androgen-insensitive CRPC cells. The 22Rv1 cells express both full-length AR and the truncated form (ARv7), whereas the C4-2 cells express only full-length AR. As controls, we performed the screens in two additional PCa cell lines: an AR positive, androgen-sensitive cell line (LNCaP), and an AR-negative cell line (PC3) (**Figure 3.1c**). For each of the four cell lines, the screens identified proteostasis factors important for growth (**Figure 3.3a**). One of the first observations was that only a small subset of proteostasis factors (~10%) was identified as “hits” in any of the cell lines. This limited sensitivity was most dramatic for the PC3 cell line, where only 4/139 (3%) genes were considered “hits” (P-value < .01; **Figure 3.3a**). This finding suggests that PC3 cells, and to a lesser extent the other cell lines, can tolerate partial loss of many/most proteostasis factors; however, because this is a pooled screen, it also remains likely that there are also false negatives. Regardless, the low percentage of “hits” allowed us to rapidly focus on the most sensitive factors.

To explore the similarities and differences between the cell lines in more detail, we established a cut-off of P-value < .01 ($-\log_{10}$(P-value) > 2) and then combined the vulnerabilities from the CRPC (22Rv1 and C4-2) cell lines and compared them to the LNCaP cell lines. At this point, the PC3 data was excluded due to the low hit rate. This comparative analysis identified 17 “hits” that are largely shared across the cell lines (*e.g.* shared vulnerabilities), as well as 3 unique vulnerabilities for the LNCaP cells and 11 hits unique to CRPC (**Figure 3.3b**). The shared vulnerabilities included a subset of Hsp70s and Hsp40/JDPs, as well as TriC/CCT, Hsp10 (gene name HSPE1) and VCP/p97 (**Figure 3.3b**). This result was satisfying because, as mentioned above, Hsp70s, Hsp90s, and JDPs, have a well-characterized role in AR processing (*24-26*). Interestingly, these AR processing factors were not identified in the PC3 cell line, which does not express AR or ARv, but were shared in the LNCaP, 22Rv1 and C4-2 cell lines which do (see Fig 1C). It seems likely that some of the other shared factors are involved in general cancer cell growth and survival, and indeed, VCP/p97, has been previously identified as being broadly important in prostate cancer (*41*).

Next, to better visualize the selective vulnerabilities, we plotted the $-\log_{10}$P for each gene in the LNCaP experiments vs. each of the two CRPC cell lines (**Figure 3.3c**). We also plotted the sensitivities onto the shRNA library maps to look for physical/functional relationships (**Figure 3.4**). Through this analysis, we observed that the LNCaP cells appear to have a reliance on HSPA4 (an Hsp70 isoform) and PTGE53 (p23), the latter of which has been associated with both Hsp90-dependent and independent roles in

transcription (*42, 43*). Next, we turned our attention to the factors that were identified as selective vulnerabilities in the CRPC cells. Most strikingly, this analysis showed that 22Rv1 and C4-2 cells depend on the mitochondrial chaperone, Hsp60. Hsp60 is known to form a complex in the mitochondria with Hsp10/HSPE1, which is a shared hit among all 4 tested cell lines. The C4-2 cells also depended on GrpEL1, another mitochondria-localized chaperone that is thought to be involved in mitochondrial protein folding and import. Together, these results suggested that CRPC cells have selective vulnerabilities in the proteostasis network and that a number of these cluster to the mitochondrial sub-network.

Synthetic lethality screens with Hsp70 and Hsp90 inhibitors highlight Hsp60 as an important selective vulnerability in CRPC cells. Because Hsp70 and Hsp90 are known to be involved in AR processing, we wondered whether repeating the shRNA screens in the presence of chemical inhibitors of these chaperones might reveal synthetic lethalities. First, we characterized the effects of these inhibitors on AR and ARv in our hands. Consistent with the literature (*28*), we found that treatment with AUY-922 (an inhibitor of Hsp90; **Figure 3.5a**) leads to loss of full length (FL) AR in 22Rv1, LNCaP, and C4-2 after 6 hours (**Figure 3.5b**). We also confirmed that AUY922 was unable to affect the variant AR (ARv) in 22Rv1 cells. On the other hand, treatment with JG-231 (an inhibitor of Hsp70) only mildly reduced FL AR, but was effective in reducing ARv in the 22Rv1 cells (**Figure 3.5b**).

Guided by these results, we repeated the shRNA screen in the 22Rv1, C4-2 and LNCaP cell lines in the presence of JG-231 or AUY-922. Cells were treated three times throughout the growth period with either JG-231 or AUY-922, at established concentrations that were found to have anti-proliferative effects while still allowing cells to recover and continue growing (see Methods). Through the calculations described earlier, we determined the phenotype and P value of genetic knockdown in each of these conditions. We found that the main "hits" from these chemical-genetic screens could be binned into 3 categories – shared, cell-line specific, and drug-treatment specific. Among the shared and cell-line specific hits, we found that the vulnerabilities were largely similar between the initial screen and the chemical-genetic screen. For example, Hsp70 isoforms (gene name HSPA8, HSPA9, HSPA14), the JDPs (DNAJA3, DNAJC8), and the TRiC complex (CCT4, CCT7, CCT8) remain essential in the presence of either inhibitor (**Figure 3.5c**). Consistent with this idea, hierarchical clustering revealed overall, similar patterns of genetic vulnerabilities (**Figure 3.6**). However, novel hits emerged as well. For example, we found that two cytosolic Hsp90 genes (HSP90AA1 and HSP90AB1) are essential in the presence of the Hsp90 inhibitor (AUY-922) in all three cell lines. Moreover, HSP90AB1 was also essential in 22Rv1 cells after Hsp70 inhibition. These strong interactions suggested, perhaps not surprisingly, that the proteostasis network becomes more reliant on Hsp90s when this chaperone is partially inhibited. Interestingly, the co-chaperone HOP/STIP1, which is known to bind both Hsp70 and Hsp90 (*44, 45*), was also only required in the presence of AUY-922. This result suggests that the communication between these chaperones might become more important upon Hsp90 inhibition. Another striking finding from this

synthetic lethal screen was that Hsp60/HSPD1 was again found to be a strong vulnerability only in the 22Rv1 and C4-2 cells, but not the LNCaP (**Figure 3.5c**). Overall, these results validated our previous observations and suggested that Hsp60 could be an interesting target in CRPC cells.

Hsp60 is a selective vulnerability in CRPC cells. Hsp60 is a mitochondrial chaperonin, homologous to the bacterial GroEL, which is involved in mitochondrial protein folding (*46, 47*). To validate the Hsp60 result from the screen, we transduced 22Rv1, C4-2, LNCaP and PC3 cells with 2 different RFP-labeled shRNAs or a scrambled negative control, and selected with puromycin. In 22Rv1 cells, knockdown was >90% for both shRNA sequences, but not the control (**Figure 3.7a**). The cells were then maintained for 3 weeks and the percentage of RFP-positive cells was monitored during every passage by flow cytometry (**Figure 3.8**). From these studies, we observed depletion of the RFP-positive population in the 22Rv1 (**Figure 3.7b**) and C4-2 cells, but not LNCaP or PC-3 cells (**Figure 3.7c**). To understand whether this reliance on Hsp60 was restricted to CRPC cell lines, we knocked it down in multiple other cancer subtypes. Here, we focused on breast cancer (MCF7 and MDA-MD-231) and multiple myeloma (KMS-11, KMS-34, OPM-2, AMO-1) cell lines, due to their established connection with chaperones and proteostasis (**Figure 3.8**) (*48, 49*). We found that 4/6 cell lines did not rely on Hsp60/HSPD1 for growth (**Figure 3.7c**). In 2/6 cell lines (MCF-7 and KMS-34), only a partial decrease (about 50% depletion compared to the control) in the RFP population was observed. Thus, the CRPC cell lines had an unusual, but not entirely exclusive, reliance on Hsp60/HSPD1.

Hsp60 knockdown does not affect AR levels. While Hsp70 and Hsp90 directly regulate AR stability (see Fig 3B), we considered it unlikely that Hsp60 would operate through a similar mechanism due to it's mitochondrial localization. However, the expression of AR and ARv7 is known to be sensitive to manipulation of metabolic pathways, such as inhibition of fatty acid metabolism (*50, 51*), so it seemed possible that Hsp60 could regulate AR stability through indirect mechanisms. Thus, we examined whether Hsp60 knockdown reduced AR levels in the dox-inducible 22Rv1 cells. These cells were treated with dox for 96 hours, which produced a robust knockdown of Hsp60 without any impact on AR or ARv (**Figure 3.9a**). These results suggest that Hsp60 is involved in survival of CRPC cells through a mechanism that is independent of AR stability.

Metabolic effects of Hsp60 KD. Another possibility is that Hsp60 could be important for metabolic reprogramming in CRPC cell lines. To test this idea, we monitored the impact of Hsp60 loss on mitochondrial respiration in 22Rv1 cells using the Mito Stress Test (Agilent). In this assay, oligomycin, trifluoromethoxy carbonylcyanide phenylhydrazone (FCCP), and Rotenone/Antimycin A are sequentially added to cultured cells to calculate mitochondrial activity and capacity (**Figure 3.9b**). Upon 5-day treatment with dox, Hsp60-knockdown suppressed numerous aspects of mitochondrial respiration. In general, Hsp60 loss resulted in lower basal oxygen consumption; however, this effect was relatively minor compared to the decrease in the maximal oxygen consumption rate (OCR; **Figure 3.9c**). Loss of Hsp60 consistently reduced the

spare respiratory capacity (maximal OCR – basal OCR) of 22Rv1 cells and was generally accompanied by an increase in proton leakage, an indication that the integrity of the electron transport chain (ETC) and/or the inner membrane are disrupted (**Figures 3.9e and 3.9f**). These effects were often accompanied by variable impacts on basal respiration and glycolytic response, indicating that Hsp60 is more important in maintaining mitochondrial plasticity than it is in maintaining basal respiration in 22Rv1 cells (**Figure 3.9d**).

Clinical significance of Hsp60 in CRPC. Lastly, we wanted to examine if Hsp60 expression had a clinical correlation to patient outcomes in prostate cancer, and especially in those individuals who had been previously treated with ADT. Towards that goal, we analyzed metastasis-free survival in ADT-treated (n=243) and non-ADT treated (n=476) patients by comparing based on Hsp60/HSPD1 gene transcript levels. Here, high Hsp60 expression was defined as greater than the median of all patients. Strikingly, ADT-treated patients with high Hsp60 expression had significantly worse outcomes (**Figure 3.10**, HR=1.95, p = 0.00024). In the patients who had not received ADT (no-ADT), those with high Hsp60 expression have slightly worse metastasis-free survival outcomes (HR=1.4), but this finding was not statistically significant. These findings suggest that high Hsp60 levels correlate with worse metastasis-free survival in prostate cancer patients, especially in those patients previously treated with ADT.

Discussion

Given the established dependence of prostate cancer cells on AR, the proteostasis network has been suggested to contain putative drug targets (*52*). Here, we used focused shRNA screens to identify factors that might be required for cell growth and survival in CRPC and PCa cell lines. Through these studies, we discovered “hits” that are shared amongst all the cell lines, such as the TriC/CCT complex, VCP/p97, and Hsp10. Both TriC/CCT and VCP/p97 have been broadly implicated in tumorigenesis (*53, 54*), so this shared dependence was consistent with probable roles in sustaining general cancer phenotypes, such as rapid growth and proliferation. Here, we were more interested in those factors that were selective for growth of individual cell lines. Among all of the findings, we became most interested in Hsp60/HSPD1, which was only identified as a strong hit in the CRPC cell lines (22Rv1 and C4-2). This chaperone had previously been linked to clinical prostate cancer (*55, 56*), so this finding seemed most promising.

Hsp60 is known to be involved in mitochondrial protein folding and translocation (*46, 47*). It has been shown to have various roles in cancer, such as glioblastoma (*57, 58*), but its exact function has not been determined. Proteomics studies have identified a number of substrates of Hsp60, including malate dehydrogenase and other TCA cycle-related proteins (*59*). We found that knockdown of Hsp60/HSPD1 does not affect AR levels, but rather has a strong effect on mitochondrial spare respiratory capacity (**Figure 3.9d**). Spare respiratory capacity is a strong predictor of metastatic potential, given that it is related to a cell’s ability to respond to diverse stress stimuli (*60*). As cancer cells

escape their tissue of origin, they encounter environments that differ substantially from the nutritional characteristics to which they are accustomed. Spare respiratory capacity likely plays an important role in supporting foreign cells' ability to thrive in such environments thereby promoting prostate cancer ability to escape it's natural environment and thrive in foreign nutrient environments. Our results support a model in which prostate cancer becomes increasingly reliant on Hsp60 as it deviates from androgen-dependent growth and escapes the prostate. By promoting the activity of components of the ETC, Hsp60 helps CRPC cells weather the stress related to metastatic growth. This relationship appears to be important in patients, as we observed in clinical data that Hsp60 expression significantly correlates with metastasis-free survival in prostate tumors from patients treated with ADT. Moreover, Hsp60 is upregulated after 8 weeks in a mouse model of CRPC development (*61*). These findings generally agree with our *in vitro* observations that Hsp60 plays a special role in CRPC cell lines, but not LNCaP or PC3. Hsp60 (and its prokaryotic ortholog, GroEL, has been the target of multiple drug discovery and chemical biology campaigns (*57, 62-65*). The present study suggests that CRPC might be a promising disease target for these emerging inhibitors.

More broadly, it seems likely that the proteostasis networks of prostate cancer cells are re-programmed during disease progression and the onset of ADT resistance. Thus, whether an inhibitor of proteostasis works for a specific prostate cancer stage might depend on multiple factors, including the prior treatment regime. Functional genetic tools such as the Proteostasis Library, plus other biochemical technologies (*9, 66, 67*),

may begin to unravel these selective vulnerabilities for prostate cancer and other indications.

Methods

Cell lines

PC3, LNCaP, C4-2, and 22Rv1 cells were purchased from ATCC and grown in RPMI 1640 medium supplemented with 10% non heat-inactivated fetal bovine serum (Gibco 16000044) and 1% penicillin/streptomycin. All cell lines were maintained in regular tissue culture-treated flasks, with the exception of the low-adherent LNCaPs, which were kept in carboxyl-coated flasks (Corning 354778). All cells were grown at 37 °C and 5% CO_2.

Reagents

JG-231 was prepared in house, as described (*68*). AUY-922 was purchased from Advanced ChemBlocks Inc. (cat # 10274). The chaperone shRNA library was prepared as previously described (*33*). Briefly, sequences were cloned into the lentiviral backbone plasmid, pMK1275. For verification, individual shRNAs were cloned into either the dox-inducible backbone, pMK1201 (derived from pINDUCER10 of the Elledge Lab) or pMK1200.

Lentiviral production and transduction

All lentiviruses were prepared by transfection into HEK293T cells using Lipofectamine 2000 and packaging plasmids pMol, pRSV, and pVSV-g. Viral particles were allowed to form for 48 hours post transfection, and then the viral supernatant was collected,

passed through a 0.45 μm filter, and stored at 4 °C for no longer than one week prior to use. Viral supernatant was added to suspended cells immediately following trypsinization, along with 8 μg/mL polybrene (Santa Cruz sc-134220). The cells were allowed to adhere to the flasks, then the medium was replaced with regular growth medium after 6-8 hours. After 48 hours, the cells successfully infected with the lentiviral plasmids were selected with 1 μg/mL puromycin (Gibco A11138-03) for an additional 48 hours. Flow cytometry was used to determine infection and selection efficiency via the expression of fluorescent markers encoded by the lentiviral vectors (generally BFP for pooled shRNA screens, and mCherry or TurboRFP for individual shRNA constructs).

Pooled shRNA screens and individual shRNA validation

Lentivirus was prepared as described above of the pooled shRNA library and used to infect the prostate cancer cell lines. Most cell lines were initially infected at ~50-60% efficiency, monitored by BFP intensity, and then were further selected with puromycin to ~100%. Immediately following the selection T_0 samples, of ~4 million cells each, were collected and stored at -80 °C until genomic DNA was isolated for sequencing. The cells were continually cultured, maintaining at least 4 million cells with each passage, for a period of ~10 doublings. For screens with chaperone inhibitors, the cells were dosed three times at the concentrations listed in 3. 1, for a duration of 24 hours each time. Concentrations were chosen by determining the IC50 per cell line by MTT assay, then further optimized by testing multiple concentrations at around the IC50 and observing the effects on cells after treatment and multiple days of recovery. Final concentrations were chosen as ones that induced cell death for a sizable population, but still allowed to

cells to recover and continue growing, to reduce potential bottlenecking. At the end of the growth period, samples of ~4 million cells were collected for the T_{final} sample. For individual shRNA validation, lentivirus was prepared as described, cells were transduced and monitored by RFP intensity. Cells were then further selected with puromycin, so the final population was 50-80% RFP-positive. The percentage of RFP positive cells was then monitored by flow cytometry over a ~2 week period, with cells being split at a 1:4 ratio whenever confluency was reached.

Table 3.1. Compounds and concentrations used in the shRNA screens.

	Screen conditions	
Cell Line	JG231 (uM)	AUY (nM)
22Rv1	0.75	100
PC3	0.5	100
LNCaP	1	100
C4-2	1	100

Genomic DNA isolation, indexing and PCR purification

Genomic DNA was extracted using MN NucleoSpin® Blood Kit (Macherey-Nagel 740951) for ~4-6 million cells per sample. Whole genomic DNA samples were carried forward into indexing PCRs using Q5® High-Fidelity polymerase (New England BioLabs M0492S). PCR amplified, and indexed, fragments of approximately 280 bp were purified by a two-step SPRI bead purification (43), and concentrations were determined on a Qubit Fluorometer before pooling for deep sequencing on a HiSeq 4000.

Mito Stress Test

Stable 22Rv1 cells containing dox inducible-expressing shRNA constructs (shRNA-

Hsp60-1 or Hsp60-2) were stimulated with 100 ng/mL doxycycline for 4 days prior to seeding 2.0 x 10^4 cells/well in a 96 well plate. Oxygen consumption (OCR) and extracellular acidification rate (ECAR) were monitored with Agilent SeaHorse XFe96 ~18h after seeding with XF DMEM pH 7.4 containing glucose, pyruvate, and glutamine. All experiments were normalized by DNA quantification with Cyquant (ThermoFisher) and are the result of at least 4 replicates per condition. Spare respiratory capacity (maximal OCR – basal OCR) and proton leakage (oligomycin-sensitive OCR – non-mitochondrial OCR) were calculated using Wave (Agilent).

Data Analysis and Clustering

Gene were clustered hierarchically by P value in Cluster, as described (*69*) and displayed by Java TreeView (*70*).

Immunoblotting

Cells were grown in a 6-well plate to near 100% confluency, after which the medium was replaced with fresh medium containing the compounds in 1% DMSO. The compound was left on the cells and incubated at 37 °C and 5% CO_2 for six hours, immediately followed by harvesting and lysing in M-PER supplemented with protease inhibitors. Lysate concentrations were quantified by a bicinchoninic acid assay (BCA, ThermoFisher 23227) and then run on 4-15% gradient SDS polyacrylamide gels at 5-10 µg of total protein per sample. All blot quantification was performed in Image Lab™ software (BioRad). The following antibodies were used:

Table 3.2. List of antibodies and dilutions used for Western blot studies.

Target	Company/Cat #	Dilution used	Host
AR	Abcam (ab133273)	1:1000	Rabbit
Hsc/p70	San Cruz (sc33575)	1:200	Rabbit
Hsp27	Santa Cruz (sc59562)	1:200	Mouse
Hsp60	Cell Signaling (D6F1)	1:1000	Rabbit
Hsp10	Santa Cruz (sc376313)	1:1000	Mouse
Actin	Sigma (A5441)	1:200	Mouse

Clinical data analysis

Expression profiles of retrospective radical prostatectomy samples from 719 patients (243 with ADT treatment, 476 no treatment) were retrieved from Decipher GRID database. Patients cohort was pooled from two matched cohort previously for building and validating ADT signature designed as described in (PMID 29760221). Specimen selection and processing and data normalization has been described previously (PMID 29760221). Patients were grouped based on expression of HSP60. High HSP60 was defined as higher than median expression.

Figures

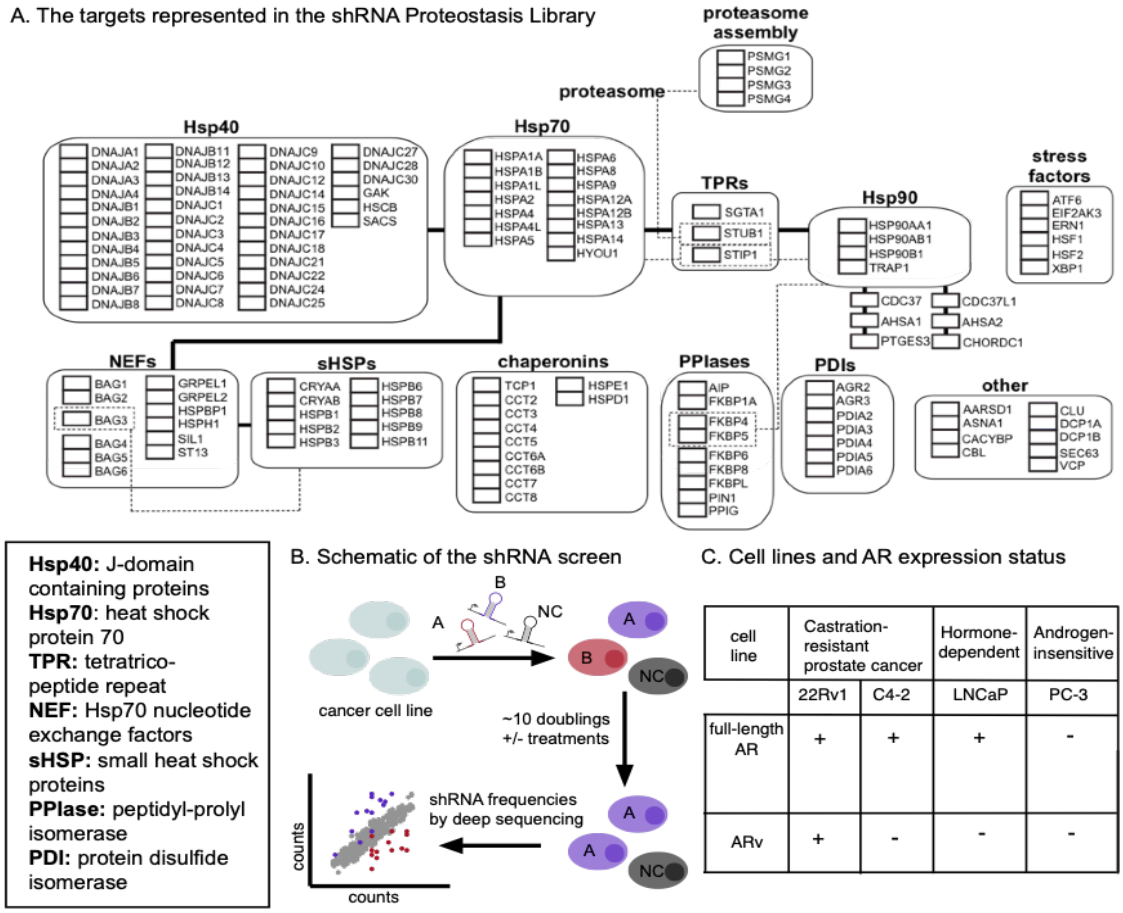

cell line	Castration-resistant prostate cancer		Hormone-dependent	Androgen-insensitive
	22Rv1	C4-2	LNCaP	PC-3
full-length AR	+	+	+	-
ARv	+	-	-	-

Figure 3.1 Functional genomic screen in PCa cell lines. A. Map of the chaperones and other proteostasis targets represented in the shRNA Proteostasis Library. Targets are grouped by structural categories (e.g. Hsp70s, sHSPs). The bold lines between the categories represent known physical connections (e.g. protein-protein interactions). The dotted lines represent connections that are specific to only the indicated members of the class. B. Schematic of the workflow for the functional genomics screen. Cells are transduced with lentivirus expressing targeting (A, B, etc.) and ~500 non-targeting negative control (NC) sequences. After selections performed with or without proteostasis stressors, the enrichment or depletion of specific shRNA sequences is quantified by deep sequencing and comparison of T0 to Tfinal. C. Four prostate cancer cell lines, organized by hormone sensitivity and AR expression status.

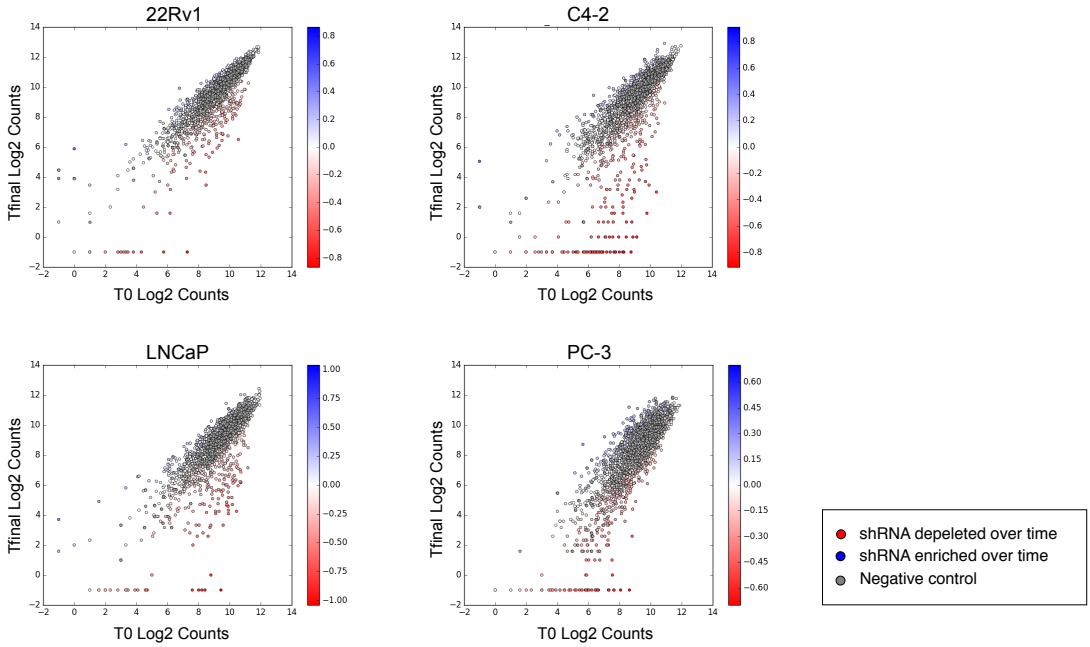

Figure 3.2. Individual shRNA results of the genetic screen in PCa cells. Barcoded shRNAs were deep sequenced at the T0 (initial) and Tfinal points and their frequencies were compared to determine phenotype of genetic knockdown. Each dot represents a single shRNA or negative control shRNA.

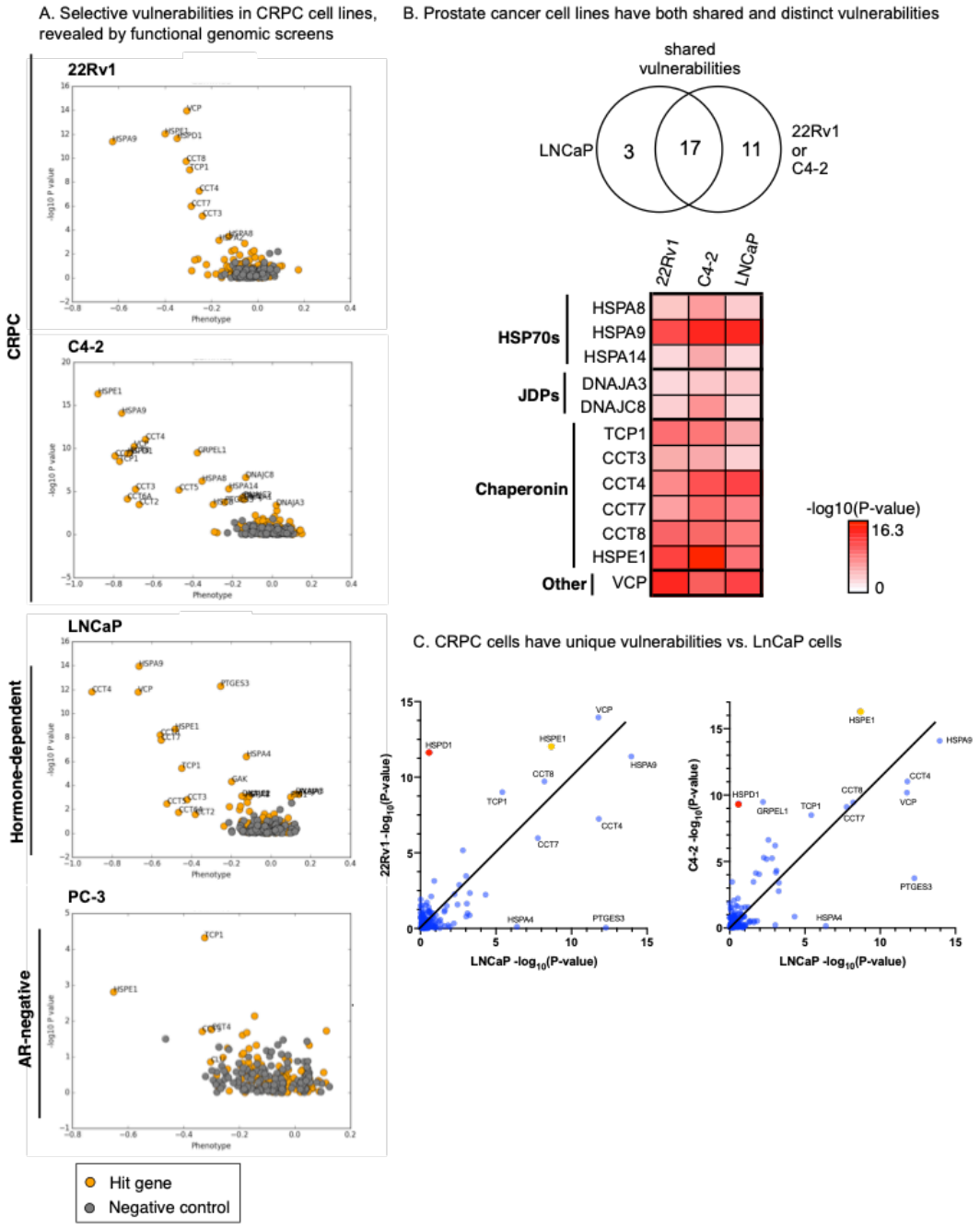

Figure 3.3. CRPC cell lines have unique vulnerabilities that are distinct from PCa cells. A. Volcano plots, showing the results of the functional genomics screen for each of the four cell lines. B. Comparisons between the CRPC cell lines (22Rv1 and C4-2) and the PCa cell lines (LNCaP) reveals both shared and distinct subsets of vulnerabilities. All genes with -log10(Pvalue) >2 in all 3 cell lines are shown. C. Comparisons between LNCaP and the CRPC cell lines.

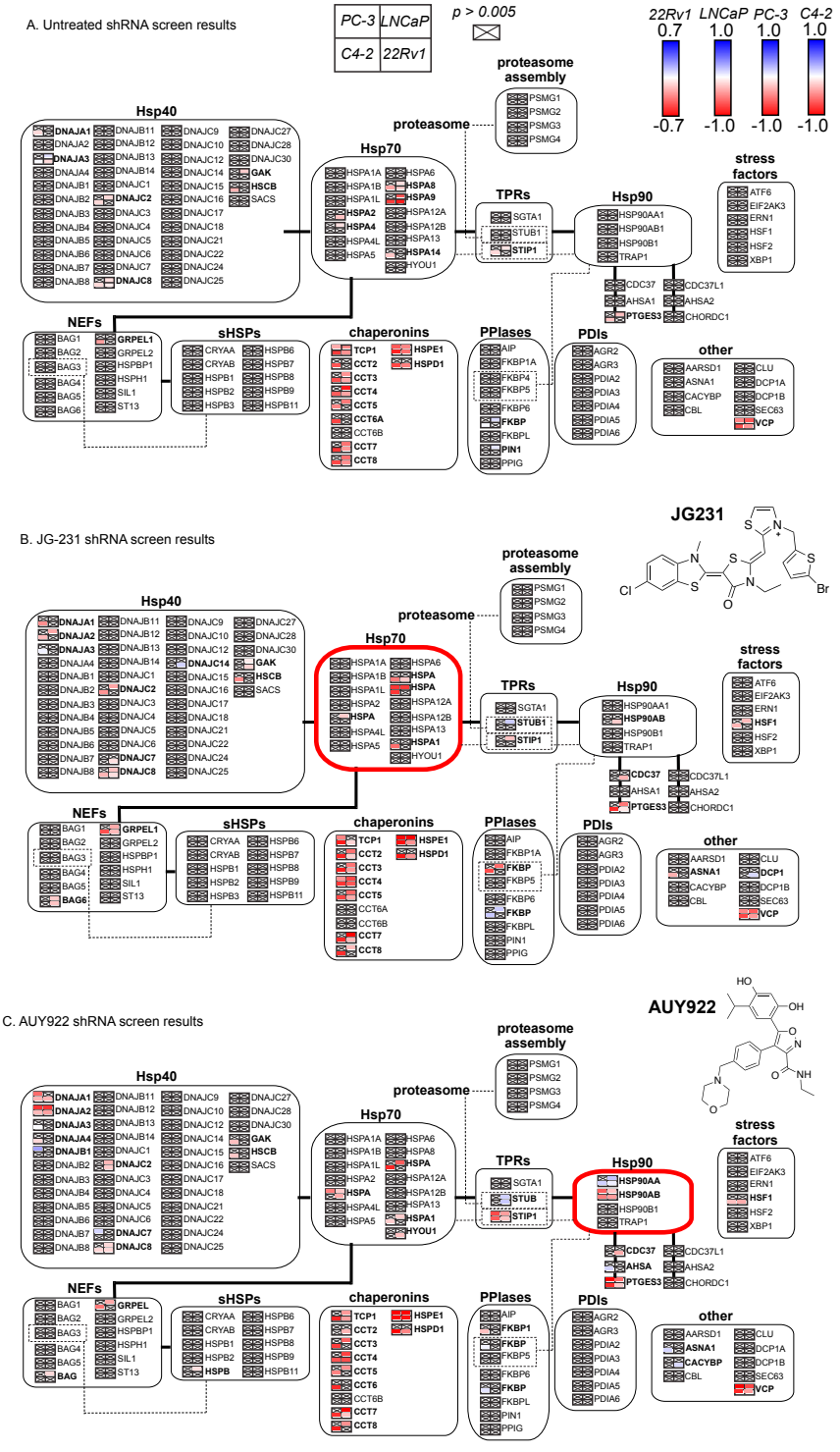

Figure 3.4 Gene level results from shRNA screens under the following conditions: untreated (A), JG-231 (B), or AUY922 (C). Chaperonins and Hsp70 genes are commonly essential. Under Hsp70 inhibition, additional Hsp70, Hsp40 and NEF genes are essential. With Hsp90 inhibition, Hsp40, Hsp70, and Hsp90 genes are essential.

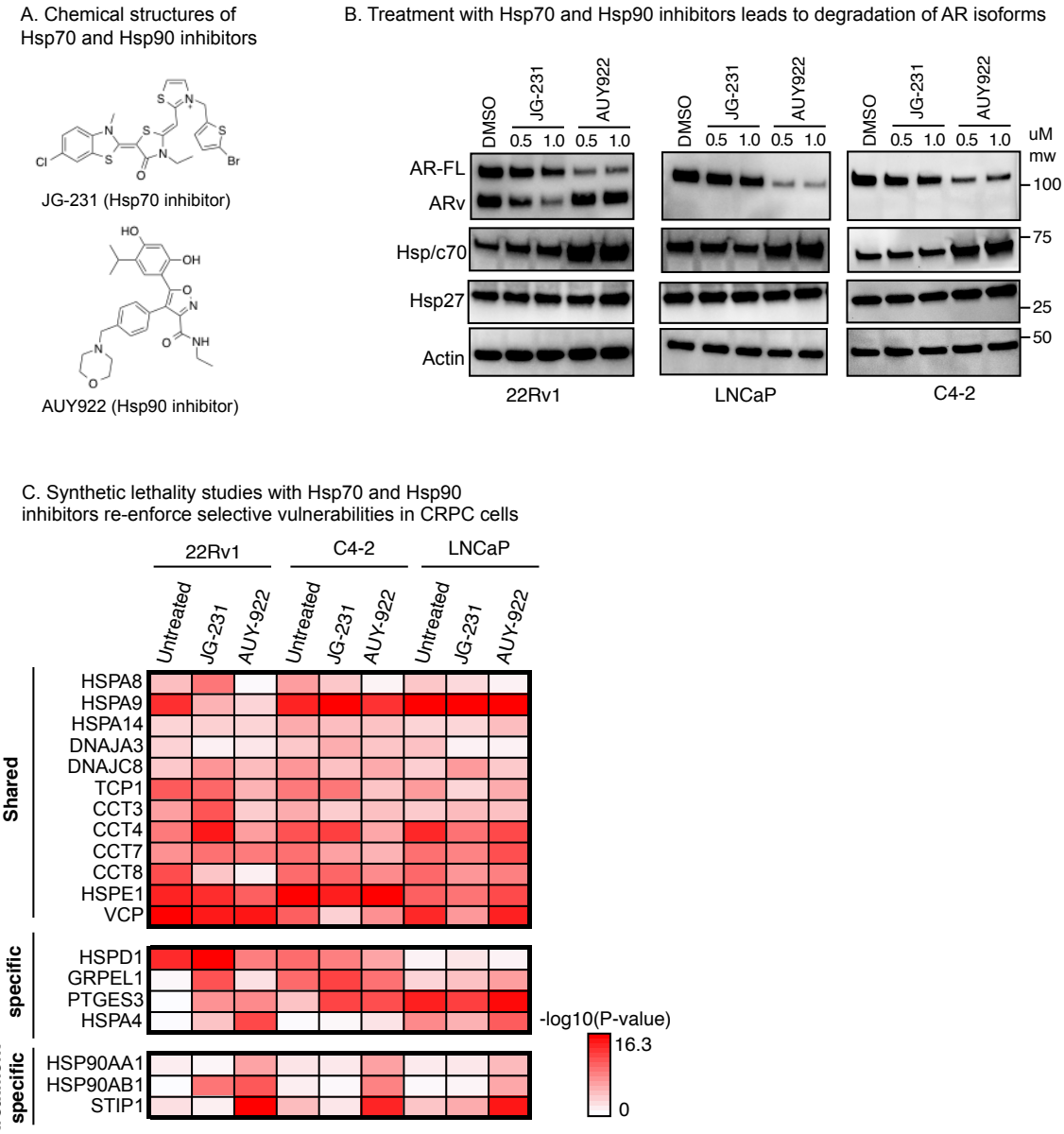

Figure 3.5. Synthetic lethality studies, using chemical inhibitors of Hsp70 and Hsp90, suggest that CRPC cells depend on Hsp60/HSPD1. A. Chemical structure of the compounds used in this study. JG-231 and AUY-922 are pan-inhibitors of Hsp70 and Hsp90, respectively. B. Treatment with AUY922 leads to degradation of full-length AR and treatment with JG-231 leads to degradation of ARv in prostate cancer cell lines. Experiments are representative of studies performed in triplicate. C. P-value of selected genes show various patterns of knockdown sensitivity across prostate cancer cells. Shared and cell line specific "hits" from the untreated condition generally remain hits with Hsp70 and Hsp90 inhibition, and some drug-treatment specific sensitivities are revealed.

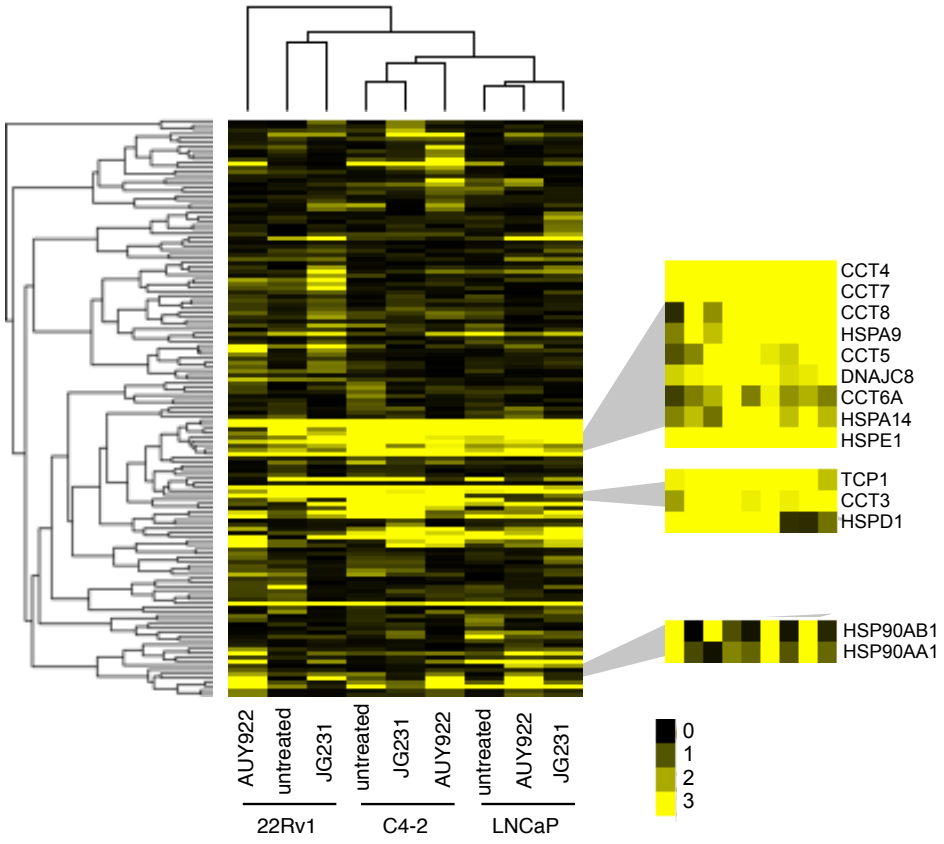

Figure 3.6. Hierarchical clustering of the p-value for targeted genes in the 22Rv1, C4-2 and LNCaP cells. Functionally related genes cluster together and re-capitulate the results observed in the untreated shRNA screen. The highligheted regions show the shared chaperonin hits (CCT genes), Hsp60 (HSPD1), which is selective for the CRPC cells, and Hsp90, which is drug-treatment specific.

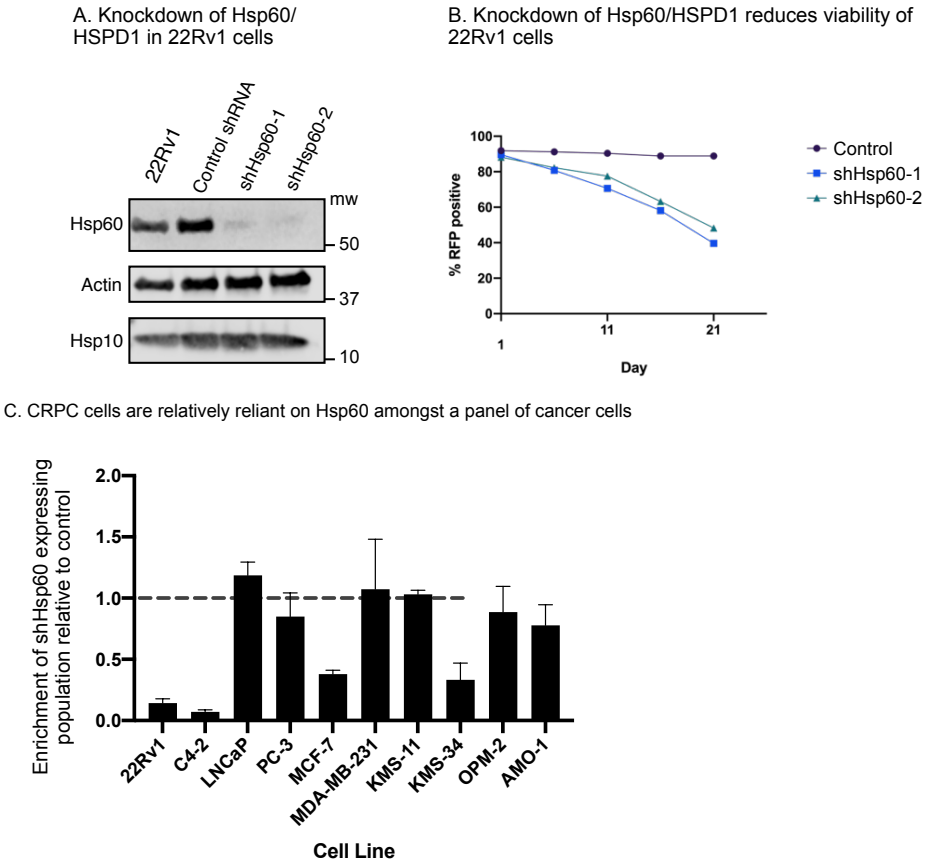

Figure 3.7. Validation of Hsp60 as a selective vulnerability in CRPC cell lines. A. 22Rv1 cells were transduced with either a control or Hsp60 targeting shRNA, which induced robust knockdown (>90%). B. The shRNA expressing population was monitored via flow cytometry through RFP expression. Over time, the population of Hsp60 knockdown cells decreased compared to the control shRNA. C. A panel of additional cancer cells were transduced with the Hsp60 shRNAs and the RFP-expressing population was monitored over time (~2-3 weeks). Hsp60 knockdown was strongly depleted in CRPC cells (22Rv1 and C4-2), but not in the other tested PCa, breast, or multiple myeloma cells. Enrichment was calculated as the ratio of (RFP+)/(1-RFP+) between the initial and final time point, relative to a control shRNA.

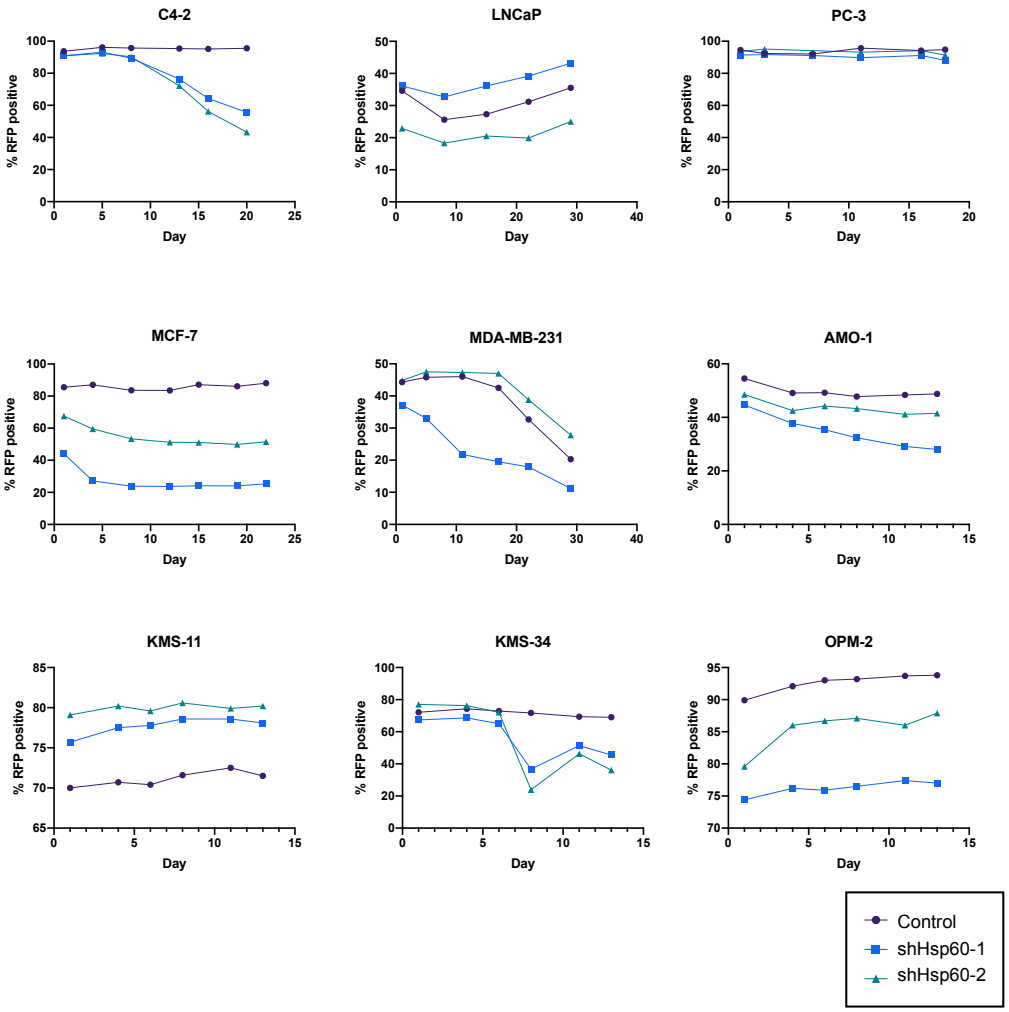

Figure 3.8 Cells from various tissue types (prostate, breast, and multiple myeloma) were transduced with either a control or Hsp60 targeting shRNA with an RFP marker. The shRNA expressing population was monitored over time (~2-3 weeks) via flow cytometry.

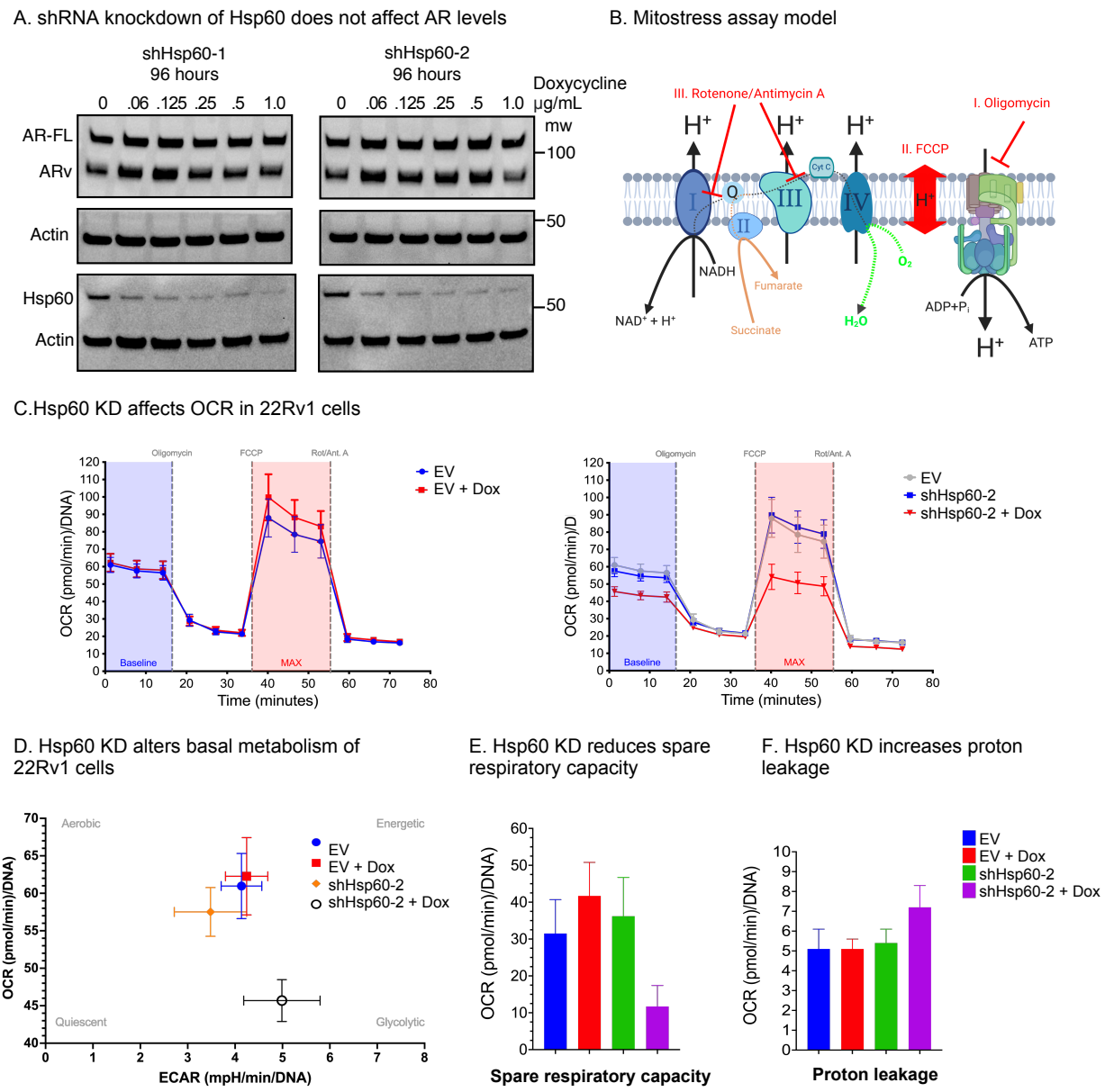

Figure 3.9. Hsp60 knockdown does not affect AR but Hsp60 promotes mitochondrial respiration of 22Rv1 cells. A. Dox-inducible shRNAs of Hsp60 were stably expressed in 22Rv1 cells. shRNAs reduce Hsp60 levels, but both full-length and ARv levels are unaffected after 96 hr dox treatment. B. Model of mitostress assay overlayed on inner mitochondrial membrane and ETC. C. Mitostress analysis of 22Rv1 EV or dox-inducible shHsp60-2 +/- 5 day treatment with 100 ng/mL doxycycline. D. Energyetic plot of basal metabolism of 22Rv1 EV or shHsp60-2 cell with and without doxycycline. E. Quantitation of spare respiratory capacity or F. proton leakage of 22Rv1 EV or Hsp60-3 +/- 5 day treatment with 100 ng/mL doxycycline.

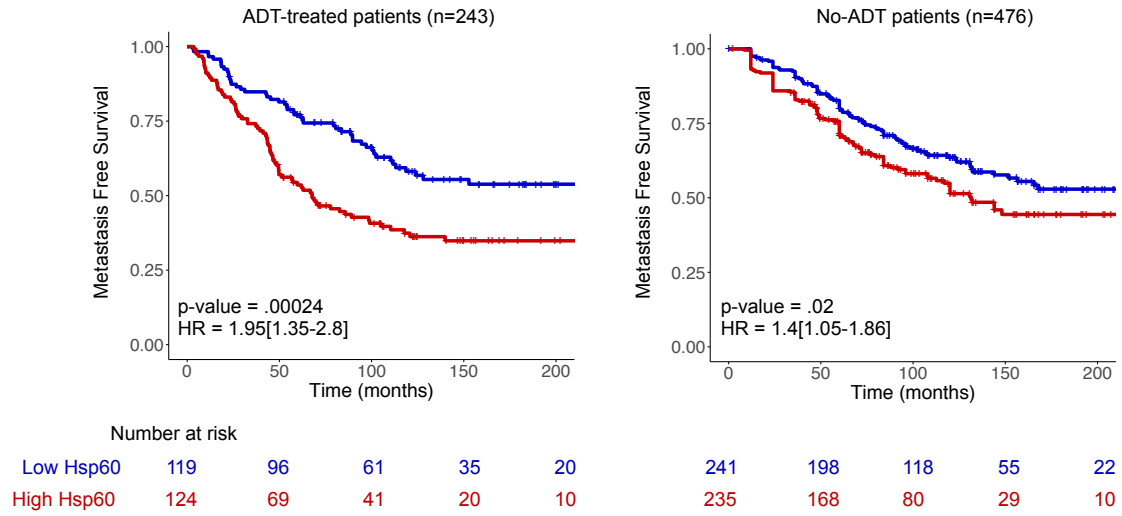

Figure 3.10: Comparison of metastasis-free survival in patients with high (red, greater than median expression) or low (blue, lower than median expression) Hsp60 expression, with or without ADT treatment. Hsp60 expression significantly correlates with worse outcomes in ADT-treated prostate cancer patients.

References

1. W. E. Balch, R. I. Morimoto, A. Dillin, J. W. Kelly, Adapting proteostasis for disease intervention. *Science* **319**, 916-919 (2008).
2. J. L. Brodsky, G. Chiosis, Hsp70 molecular chaperones: emerging roles in human disease and identification of small molecule modulators. *Curr Top Med Chem* **6**, 1215-1225 (2006).
3. S. Chaudhury, T. R. Welch, B. S. Blagg, Hsp90 as a Target for Drug Development. *ChemMedChem*, (2006).
4. M. V. Powers, P. A. Clarke, P. Workman, Death by chaperone: HSP90, HSP70 or both? *Cell Cycle* **8**, 518-526 (2009).
5. L. Whitesell, S. L. Lindquist, HSP90 and the chaperoning of cancer. *Nature reviews* **5**, 761-772 (2005).
6. R. Nagel, E. A. Semenova, A. Berns, Drugging the addict: non-oncogene addiction as a target for cancer therapy. *EMBO Rep* **17**, 1516-1531 (2016).
7. J. Luo, N. L. Solimini, S. J. Elledge, Principles of cancer therapy: oncogene and non-oncogene addiction. *Cell* **136**, 823-837 (2009).
8. L. J. Crawford, B. Walker, A. E. Irvine, Proteasome inhibitors in cancer therapy. *Journal of cell communication and signaling* **5**, 101-110 (2011).
9. A. Rodina *et al.*, The epichaperome is an integrated chaperome network that facilitates tumour survival. *Nature* **538**, 397-401 (2016).
10. P. K. Wu *et al.*, Mortalin (HSPA9) facilitates BRAF-mutant tumor cell survival by suppressing ANT3-mediated mitochondrial membrane permeability. *Science signaling* **13**, (2020).

11. V. L. Gabai *et al.*, Anticancer Effects of Targeting Hsp70 in Tumor Stromal Cells. *Cancer Res* **76**, 5926-5932 (2016).

12. S. K. Calderwood, J. Gong, Heat Shock Proteins Promote Cancer: It's a Protection Racket. *Trends Biochem Sci*, (2016).

13. C. A. Heinlein, C. Chang, Androgen receptor in prostate cancer. *Endocr Rev* **25**, 276-308 (2004).

14. M. Kirby, C. Hirst, E. D. Crawford, Characterising the castration-resistant prostate cancer population: a systematic review. *Int J Clin Pract* **65**, 1180-1192 (2011).

15. C. J. Logothetis *et al.*, Molecular classification of prostate cancer progression: foundation for marker-driven treatment of prostate cancer. *Cancer Discov* **3**, 849-861 (2013).

16. C. S. Grasso *et al.*, The mutational landscape of lethal castration-resistant prostate cancer. *Nature* **487**, 239-243 (2012).

17. P. A. Watson, V. K. Arora, C. L. Sawyers, Emerging mechanisms of resistance to androgen receptor inhibitors in prostate cancer. *Nature reviews* **15**, 701-711 (2015).

18. D. A. Quigley *et al.*, Genomic Hallmarks and Structural Variation in Metastatic Prostate Cancer. *Cell* **175**, 889 (2018).

19. E. S. Antonarakis *et al.*, AR-V7 and resistance to enzalutamide and abiraterone in prostate cancer. *N Engl J Med* **371**, 1028-1038 (2014).

20. R. B. Montgomery *et al.*, Maintenance of intratumoral androgens in metastatic prostate cancer: a mechanism for castration-resistant tumor growth. *Cancer Res* **68**, 4447-4454 (2008).

21. M. Puhr *et al.*, The Glucocorticoid Receptor Is a Key Player for Prostate Cancer Cell Survival and a Target for Improved Antiandrogen Therapy. *Clin Cancer Res* **24**, 927-938 (2018).

22. V. K. Arora *et al.*, Glucocorticoid receptor confers resistance to antiandrogens by bypassing androgen receptor blockade. *Cell* **155**, 1309-1322 (2013).

23. C. E. Massie *et al.*, The androgen receptor fuels prostate cancer by regulating central metabolism and biosynthesis. *EMBO J* **30**, 2719-2733 (2011).

24. W. B. Pratt, Y. Morishima, M. Murphy, M. Harrell, Chaperoning of glucocorticoid receptors. *Handb Exp Pharmacol*, 111-138 (2006).

25. E. Kirschke, D. Goswami, D. Southworth, P. R. Griffin, D. A. Agard, Glucocorticoid receptor function regulated by coordinated action of the Hsp90 and Hsp70 chaperone cycles. *Cell* **157**, 1685-1697 (2014).

26. P. C. Echeverria, D. Picard, Molecular chaperones, essential partners of steroid hormone receptors for activity and mobility. *Biochim Biophys Acta* **1803**, 641-649 (2010).

27. W. B. Pratt, D. O. Toft, Regulation of signaling protein function and trafficking by the hsp90/hsp70-based chaperone machinery. *Exp Biol Med (Maywood)* **228**, 111-133 (2003).

28. M. A. Moses *et al.*, Targeting the Hsp40/Hsp70 chaperone axis as a novel strategy to treat castration-resistant prostate cancer. *Cancer Res*, (2018).

29. L. Chen *et al.*, Cotargeting HSP90 and Its Client Proteins for Treatment of Prostate Cancer. *Mol Cancer Ther* **15**, 2107-2118 (2016).

30. J. T. De Leon *et al.*, Targeting the regulation of androgen receptor signaling by the heat shock protein 90 cochaperone FKBP52 in prostate cancer cells. *Proc Natl Acad Sci U S A* **108**, 11878-11883 (2011).

31. B. Eftekharzadeh *et al.*, Hsp70 and Hsp40 inhibit an inter-domain interaction necessary for transcriptional activity in the androgen receptor. *Nature communications* **10**, 3562 (2019).

32. J. Dong *et al.*, Hsp70 Binds to the Androgen Receptor N-terminal Domain and Modulates the Receptor Function in Prostate Cancer Cells. *Mol Cancer Ther* **18**, 39-50 (2019).

33. J. Abrams *et al.*, Functional genomics screen identifies proteostasis targets that modulate prion protein (PrP) stability. *Cell Stress Chaperones* **26**, 443-452 (2021).

34. M. Kampmann *et al.*, Next-generation libraries for robust RNA interference-based genome-wide screens. *Proc Natl Acad Sci U S A* **112**, E3384-3391 (2015).

35. M. Kampmann, M. C. Bassik, J. S. Weissman, Integrated platform for genome-wide screening and construction of high-density genetic interaction maps in mammalian cells. *Proc Natl Acad Sci U S A* **110**, E2317-2326 (2013).

36. R. Freilich, T. Arhar, J. L. Abrams, J. E. Gestwicki, Protein-Protein Interactions in the Molecular Chaperone Network. *Acc Chem Res* **51**, 940-949 (2018).

37. J. Radons, The human HSP70 family of chaperones: where do we stand? *Cell Stress Chaperones* **21**, 379-404 (2016).

38. H. H. Kampinga *et al.*, Guidelines for the nomenclature of the human heat shock proteins. *Cell Stress Chaperones* **14**, 105-111 (2009).

39. B. Chen, W. H. Piel, L. Gui, E. Bruford, A. Monteiro, The HSP90 family of genes in the human genome: Insights into their divergence and evolution. *Genomics* **86**, 627-637 (2005).

40. R. Rosenzweig, N. B. Nillegoda, M. P. Mayer, B. Bukau, The Hsp70 chaperone network. *Nature Reviews Molecular Cell Biology* **20**, 665-680 (2019).

41. Y. Tsujimoto *et al.*, Elevated expression of valosin-containing protein (p97) is associated with poor prognosis of prostate cancer. *Clin Cancer Res* **10**, 3007-3012 (2004).

42. B. C. Freeman, S. J. Felts, D. O. Toft, K. R. Yamamoto, The p23 molecular chaperones act at a late step in intracellular receptor action to differentially affect ligand efficacies. *Genes Dev* **14**, 422-434 (2000).

43. F. J. Echtenkamp *et al.*, Global functional map of the p23 molecular chaperone reveals an extensive cellular network. *Mol Cell* **43**, 229-241 (2011).

44. B. D. Johnson, R. J. Schumacher, E. D. Ross, D. O. Toft, Hop modulates Hsp70/Hsp90 interactions in protein folding. *J Biol Chem* **273**, 3679-3686 (1998).

45. K. Bhattacharya *et al.*, The Hsp70-Hsp90 co-chaperone Hop/Stip1 shifts the proteostatic balance from folding towards degradation. *Nature communications* **11**, 5975 (2020).

46. A. Pace *et al.*, Hsp60, a novel target for antitumor therapy: structure-function features and prospective drugs design. *Curr Pharm Des* **19**, 2757-2764 (2013).

47. B. Bukau, A. L. Horwich, The Hsp70 and Hsp60 chaperone machines. *Cell* **92**, 351-366 (1998).

48. S. Sannino, J. L. Brodsky, Targeting protein quality control pathways in breast cancer. *BMC Biol* **15**, 109 (2017).

49. Z. Sha, A. L. Goldberg, Multiple myeloma cells are exceptionally sensitive to heat shock, which overwhelms their proteostasis network and induces apoptosis. *Proc Natl Acad Sci U S A* **117**, 21588-21597 (2020).

50. I. R. Schlaepfer *et al.*, Lipid catabolism via CPT1 as a therapeutic target for prostate cancer. *Mol Cancer Ther* **13**, 2361-2371 (2014).

51. G. Zadra *et al.*, Inhibition of de novo lipogenesis targets androgen receptor signaling in castration-resistant prostate cancer. *Proc Natl Acad Sci U S A* **116**, 631-640 (2019).

52. P. Ballar Kirmizibayrak, B. Erbaykent-Tepedelen, O. Gozen, Y. Erzurumlu, Divergent Modulation of Proteostasis in Prostate Cancer. *Adv Exp Med Biol* **1233**, 117-151 (2020).

53. C. Boudiaf-Benmammar, T. Cresteil, R. Melki, The cytosolic chaperonin CCT/TRiC and cancer cell proliferation. *PLoS One* **8**, e60895 (2013).

54. D. J. Anderson *et al.*, Targeting the AAA ATPase p97 as an Approach to Treat Cancer through Disruption of Protein Homeostasis. *Cancer cell* **28**, 653-665 (2015).

55. C. Castilla *et al.*, Immunohistochemical expression of Hsp60 correlates with tumor progression and hormone resistance in prostate cancer. *Urology* **76**, 1017 e1011-1016 (2010).

56. D. A. Beyene *et al.*, Differential expression of Annexin 2, SPINK1, and Hsp60 predict progression of prostate cancer through bifurcated WHO Gleason score categories in African American men. *The Prostate* **78**, 801-811 (2018).

57. E. S. Polson *et al.*, KHS101 disrupts energy metabolism in human glioblastoma cells and reduces tumor growth in mice. *Science translational medicine* **10**, (2018).

58. H. Tang *et al.*, Down-regulation of HSP60 Suppresses the Proliferation of Glioblastoma Cells via the ROS/AMPK/mTOR Pathway. *Scientific reports* **6**, 28388 (2016).

59. A. S. Bie *et al.*, An inventory of interactors of the human HSP60/HSP10 chaperonin in the mitochondrial matrix space. *Cell Stress Chaperones* **25**, 407-416 (2020).

60. P. Marchetti, Q. Fovez, N. Germain, R. Khamari, J. Kluza, Mitochondrial spare respiratory capacity: Mechanisms, regulation, and significance in non-transformed and cancer cells. *FASEB J* **34**, 13106-13124 (2020).

61. S. Akamatsu *et al.*, The Placental Gene PEG10 Promotes Progression of Neuroendocrine Prostate Cancer. *Cell reports* **12**, 922-936 (2015).

62. K. Wiechmann *et al.*, Mitochondrial Chaperonin HSP60 Is the Apoptosis-Related Target for Myrtucommulone. *Cell chemical biology* **24**, 614-623 e616 (2017).

63. H. Shao, K. Oltion, T. Wu, J. E. Gestwicki, Differential scanning fluorimetry (DSF) screen to identify inhibitors of Hsp60 protein-protein interactions. *Org Biomol Chem* **18**, 4157-4163 (2020).

64. E. Chapman, G. W. Farr, K. Furtak, A. L. Horwich, A small molecule inhibitor selective for a variant ATP-binding site of the chaperonin GroEL. *Bioorg Med Chem Lett* **19**, 811-813 (2009).

65. M. Stevens *et al.*, Analogs of nitrofuran antibiotics are potent GroEL/ES inhibitor pro-drugs. *Bioorg Med Chem* **28**, 115710 (2020).

66. M. Taipale *et al.*, A quantitative chaperone interaction network reveals the architecture of cellular protein homeostasis pathways. *Cell* **158**, 434-448 (2014).

67. K. Rizzolo *et al.*, Features of the Chaperone Cellular Network Revealed through Systematic Interaction Mapping. *Cell reports* **20**, 2735-2748 (2017).

68. H. Shao *et al.*, Exploration of Benzothiazole-Rhodacyanines as Allosteric Inhibitors of Protein-Protein Interactions with Heat Shock Protein 70 (Hsp70). *J Med Chem*, (2018).

69. M. B. Eisen, P. T. Spellman, P. O. Brown, D. Botstein, Cluster analysis and display of genome-wide expression patterns. *Proc Natl Acad Sci U S A* **95**, 14863-14868 (1998).

70. A. J. Saldanha, Java Treeview--extensible visualization of microarray data. *Bioinformatics* **20**, 3246-3248 (2004).

Publishing Agreement

It is the policy of the University to encourage open access and broad distribution of all theses, dissertations, and manuscripts. The Graduate Division will facilitate the distribution of UCSF theses, dissertations, and manuscripts to the UCSF Library for open access and distribution. UCSF will make such theses, dissertations, and manuscripts accessible to the public and will take reasonable steps to preserve these works in perpetuity.

I hereby grant the non-exclusive, perpetual right to The Regents of the University of California to reproduce, publicly display, distribute, preserve, and publish copies of my thesis, dissertation, or manuscript in any form or media, now existing or later derived, including access online for teaching, research, and public service purposes.

DocuSigned by:
Arielle Shkedi
A6821ED41B0F41D...
Author Signature

8/3/2021
Date